

# Experimental and numerical investigation of the seismic response of precast wall connections

E. Brunesi<sup>1</sup> · R. Nascimbene<sup>1</sup>

Received: 11 January 2017 / Accepted: 27 May 2017 / Published online: 5 June 2017  
© Springer Science+Business Media Dordrecht 2017

**Abstract** This paper investigates the seismic response of lightly reinforced precast concrete shear walls typically used for low- to mid-rise residential systems in past and current Dutch building practice. The results of a wide set of pseudostatic cyclic tests performed on full-scale single precast panels with or without openings were examined and discussed, quantifying the sensitivity of structural response and failure mode to changes in axial load and wall geometry. Behavioral aspects of those panels were treated at a global/structural and local/sectional level, posing particular emphasis on their wall-to-foundation and wall-to-wall joints. Asymmetric push–pull tests of precast wall connections were also carried out and presented to characterize the cyclic behavior of this type of joint system under simulated seismic loading. The outcome of this large campaign of experimental tests was then used to develop and validate a simple numerical model to be integrated in a framework for large scale seismic fragility analysis of precast terraced structures built with this particular technology.

**Keywords** Prefabricated structure · Shear wall · Lightly reinforced wall · Wall-to-wall connection · Wall-to-foundation connection · Cyclic test · Numerical modeling · Seismic response

---

✉ R. Nascimbene  
roberto.nascimbene@eucentre.it

E. Brunesi  
emanuele.brunesi@eucentre.it

<sup>1</sup> EUCENTRE, European Centre for Training and Research in Earthquake Engineering, Via Ferrara 1, 27100 Pavia, Italy

## 1 Introduction

The use of precast concrete in wall and framing systems is widespread in many European (and non-European) countries, regardless of the level and the nature of seismic hazard to which they are exposed. Due to their versatility, their multipurpose potential and their low cost, plant-fabricated members have found wide application in building construction, particularly for what concerns single-story or low-rise residential and industrial buildings. Despite the vast variety of feasible structural schemes and solutions, the seismic response of all of them greatly depends on the behavior of the connection system, and the key role played by a proper design and detailing of the joints is well established in the literature [see among others (Vintzeleou and Tassios 1987; Tsoukantas and Tassios 1989; Englekirk 2003; Fédération Internationale du Béton 2008; Magliulo et al. 2014; Belleri et al. 2015; Brunesi et al. 2015a)]. In the past decade or so, extensive research was undertaken to test traditional structural layouts and connection systems in quasi-static, pseudodynamic, and dynamic fashion [see e.g. (Brunesi et al. 2015a; Bournas et al. 2013; Psycharis and Mouzakis 2012a, b; Belleri and Riva 2012; Fischinger et al. 2008; Rodríguez and Blandón 2005; Dal Lago et al. 2016)], reaffirming that systems designed without the ability to accommodate relative displacements between structural elements revealed a particularly high vulnerability. Along this line, the influence of cladding-frame interaction was also investigated more recently [among others (Biondini et al. 2013; Magliulo et al. 2015; Brunesi et al. 2015a; Belleri et al. 2016; Zoubek et al. 2016; Dal Lago et al. 2017a, b)], showing the effects of panel-to-panel and panel-to-structure joints on the seismic performance of precast buildings. Innovative prefabricated solutions revealed a promising response, whilst conventional connections behaved in a fairly poor manner, confirming the primary observations of damage collected in the aftermath of recent major earthquakes.

Similar considerations can be drawn for precast reinforced concrete (RC) wall systems, in the case that they present joints lacking properly conceived mechanical devices as seismic load transfer mechanisms. Rather than the exceedance of stress capacity in structural members, displacement incompatibility and complex interaction between them may indeed cause premature failures of poorly designed/detailed connections, which in turn may affect the overall structural integrity. Although the majority of early studies on structural walls was focused on cast in place elements [e.g. (Fintel 1995; Salonikios et al. 1999; 2000; Hidalgo et al. 2002; Dazio et al. 2009)], the use of precast concrete walls as primary lateral load resisting system in seismic regions has attracted significant attention in the last two decades (Kurama et al. 1999; Crisafulli et al. 2002; Holden et al. 2003; Rezaifar et al. 2008; Pavese and Bournas 2011; Palermo et al. 2013; Ricci et al. 2013; Kang et al. 2013; Palermo et al. 2014; Mousavi et al. 2014; Todut et al. 2014; Peng et al. 2016; Li et al. 2016), leading to progresses in research applications. In case of redundant wall-to-wall and wall-to-slab joints a bundled-tube behavior may be enhanced, additionally mitigating the drawbacks inherently related to the eventual use of lightweight low-strength concretes (Pavese and Bournas 2011; Palermo et al. 2014; Mousavi et al. 2014). The sensitivity of seismic behavior of structural walls to cutouts with various shape, size and position was also investigated extensively (Pavese and Bournas 2011; Todut et al. 2014; Li et al. 2016), and advances on the effects of wall flanges were recently made (Li et al. 2016). Of paramount importance from a structural/mechanical point of view is therefore the response of connection systems, which are usually designed for both wind-induced loads and seismic resistance according to conventional code regulations and prescriptive rules (CEN, European Committee for Standardization 2004a, b; EOTA, European

Organization for Technical Approvals 2010). Nevertheless, lack of seismic design and detailing, lack of redundancy and inadequate anchorage design and execution were proven to cause insufficient protection against earthquake-induced actions. As such, a delay in the adoption and implementation of modern seismic provisions may imply nontrivial considerations in terms of physical damage to buildings, which in turn may motivate the need for a framework that allows informed decision-making processes regarding the built environment of countries or regions that are prone to minor seismicity from tectonic earthquakes (Bommer et al. 2015).

To this aim, the seismic behavior of lightly reinforced precast concrete shear walls typical of past and current Dutch building practice for low- to mid-rise residential structures was explored in this paper, presenting the results of a wide campaign of experimental tests performed, under the sponsorship of NAM (Nederlandse Aardolie Maatschappij BV), as a part of the research program for hazard and risk of induced seismicity in Groningen. Pseudostatic in-plane cyclic tests were carried out considering a set of full-scale precast panels representative of those used for lateral load resistance in precast RC terraced buildings of that region. Hysteretic response and collapse mode were shown for each system under consideration and behavioral changes as a consequence of variations in initial axial load and wall geometry were predicted, allowing a detailed assessment of seismic vulnerabilities of their wall-to-foundation and wall-to-wall connections. A further set of panel subassemblies were then fabricated and tested assuming an asymmetric push–pull loading protocol in order to investigate the seismic performance of this type of joint systems under cyclic reversals. Deformed shapes and damage patterns for different levels of imposed displacement demand were collected, and the sensitivity of shear capacity and failure mode, as well as stiffness degradation and strength deterioration, to changes in wall thickness configuration was quantified accordingly. A simple and computationally efficient mechanical approach for numerical modeling of precast wall connections of similar type was finally proposed to be integrated in a framework for large scale seismic fragility analysis of precast terraced houses built with this particular technology.

Noteworthy is that the cyclic tests on precast panels and connections described here are the first step of a comprehensive experimental research program that will involve also the testing of a two-story full-scale specimen designed to combine several common features of this type of structures. Two nominally identical prefabricated prototypes will be tested at Eucentre Lab, one of them cyclically, in pseudostatic fashion, and the other one dynamically, on the shake table of the laboratory. Further characterization/companion tests will be also performed to specifically study aspects that may affect the behavior of such houses (i.e. wall-to-slab and wall-to-foundation connections).

## 2 Details of precast houses and their construction process

Reinforced concrete buildings in the Groningen region largely consist of wall-slab-wall structures, featuring no columns or beams, but only slabs and walls. These structures can be found in both cast-in-place (tunnel construction or not) as well as precast configurations, and this section deals with a brief overview of the main characteristics of the latter, given that (1) this typology is one of the most common forms of housing in Dutch building practice, and that (2) construction process and details of these houses look quite alien to common building practice in earthquake-prone countries.

This type of low-rise precast RC residential terraced buildings is usually constructed with precast floors, precast party/gable walls and precast walls in the longitudinal direction. As shown in Fig. 1, the precast walls are erected first and shored up by steel diagonal members; subsequently, the floor is settled on the walls and supported by steel rebars that connect the first with the second-story wall, through the floor. It is worth noticing that, however, these dowels are not always present in this type of construction scheme/technology. The most common precast floors for this structural typology are hollow core sections presenting circular voids in accordance with their moderate thickness (i.e. 200–250 mm). A thickness in the range 200–250 and 120–150 mm is typically assumed for party walls and inner leaf gable walls, respectively. Front and back façades of these multiple-unit buildings are generally cavity walls. The most common concrete grade used for these structures is C35/45 and the reinforcing steel is usually formed by a wire mesh with grade FeB500 steel and reinforcing ratios of about 0.2–0.4% (for party walls).

During the construction phase, use is made of cranes to erect and set in place the precast walls that rest directly on the foundations or on the ground floor slab, which in turn rests on the foundations (see Fig. 1). The latter option is anyway either less frequent or in non-standard configurations. Once the connections between the elements are realized, the temporary props used to ensure the stability of the structure against the horizontal wind actions are removed. As discussed later on, starter rebars are usually not present in this construction system, and the wall-to-foundation connections merely consist of mortar joints. Worthwhile to mention is that, whether starter rebars are adopted, they are not always ribbed, and, in the vast majority of the cases, their development length does not satisfy European prescriptions. Mechanical anchors and felts are used as well, the latter being provided at the bottom of the hollow core slabs, which are not necessarily connected



**Fig. 1** Examples of typical multi-unit precast RC houses and key details of the construction process

together through concrete topping. Discrete L-shaped metal restraints can sometimes be found in existing buildings to prevent the unseating of prefabricated wall-elements. Wall-to-wall joints are standardized solutions and are constituted by mechanical connections that can be either two-way or three-way anchorages, in case that two contiguous panels are linked or not with a perpendicular stability wall.

Following structural layouts and construction practices/details typical in the Netherlands, a two-story single-family terraced house was designed for vertical static loads in combination with wind-induced and crane-induced loads. Consideration of the latter action is justified by both production and construction processes (Fig. 1). To this aim, the Dutch national Annex NEN-EN 1990 (Nederlands Normalisatie-instituut 2011) of the Eurocode was mainly assumed in the simulated design process of this case-study structure in order to emulate common criteria available at the time of construction. Different types of precast panels were then extracted from the building under consideration and a total of eleven specimens were tested under pseudostatic cyclic loads. In particular, seven in-plane tests on full-scale precast wall systems and four tests on L-shaped panel subassemblies were planned to evaluate damage mechanisms and ultimate shear/flexural capacity of connections that are currently used in precast RC bearing panels of this type. Thus, it is worth noting that the present research work is chiefly concerned with seismic response assessment of precast walls and connection systems through experimental testing and numerical modeling, whilst the discussion of appropriate retrofit solutions is beyond the purpose of this paper, considering the fact that it should also be driven by challenging considerations and factors other than those mentioned herein (Bommer et al. 2015).

### 3 Cyclic tests of full-scale precast panels

The experimental program described here takes advantage of a series of seven full-scale specimens that were constructed according to common Dutch practice and tested quasi-statically under cyclic lateral loading. The set of reinforced precast concrete panels under investigation were extracted from a reference prototype that was designed emulating a typical configuration of a one-unit terraced building in the Groningen region. In Fig. 2, a series of drawings presenting elevation and plan view of the index building are provided to identify its structural scheme, as well as the prevailing geometric characteristics of the specimens that were object of the experimental activity.

Complementary design drawings outlining the section properties of each specimen in terms of member size and reinforcement layout can be found in the upcoming discussion, where the main assumptions concerning test setup and procedure were summarized. Mechanical properties of reinforcing steel and concrete were measured by means of companion characterization tests performed in compliance with current European standards (i.e. UNI EN ISO 15630-1 and UNI EN 12390-3-4-7).

#### 3.1 Classification and description of case-study specimens

The first phase of the experimental campaign includes a total of seven full-scale RC wall systems that were divided into two main groups based on the presence of an opening. Their primary characteristics and, hence, the main experimental parameters are provided in Table 1, along with the specimen nomenclature used hereafter. In addition, Figs. 3 and 4

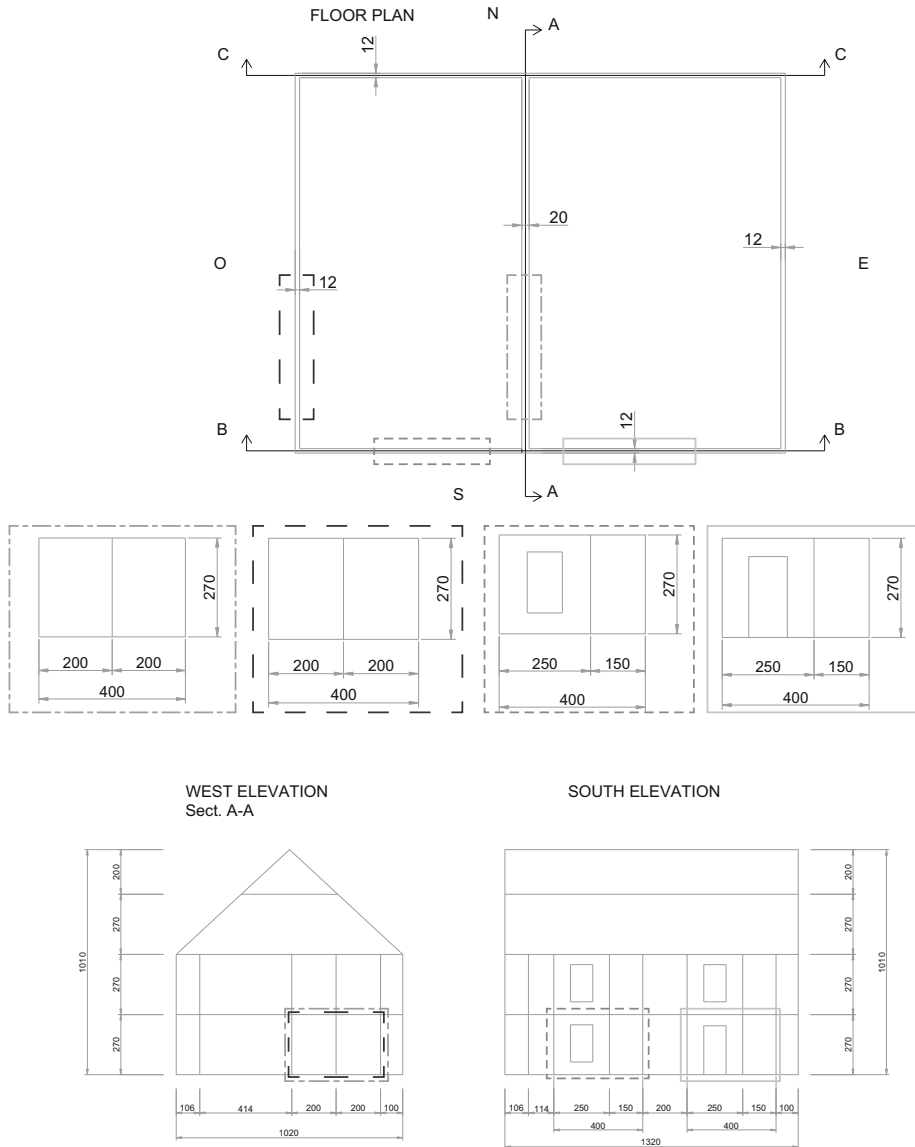


**Fig. 2** Plan and elevation view of three-dimensional reference building: representation of geometry and position of case-study structural walls

present systematic details of the structural layouts and longitudinal/transverse reinforcement arrangement considered for each type of wall.

As specified in Table 1, 200 and 120 mm thick specimens were tested under cyclic in-plane flexure with constant axial load in single bending configuration. Different values in the range 140–800 kN were assumed according to the wall thickness. In particular, as far as 120 mm thick prototypes are concerned, two axial load levels were planned for each structural configuration in order to investigate the influence of this parameter on the

**Table 1** Wall systems—specimen nomenclature and test characteristics

Specimen	Opening	Thickness (cm)	Axial load (kN)	Application (kN)	Starter rebars
SP 01	w/o	20	800	400 + 400	2Ø8
SP 02	w/o	12	500	250 + 250	w/o
SP 03	w/o	12	200	100 + 100	w/o
SP 04	Window (W)	12	360	90 + 90 + 180	w/o
SP 05	Window (W)	12	140	35 + 35 + 70	w/o
SP 06	Door (D)	12	360	90 + 90 + 180	w/o
SP 07	Door (D)	12	140	35 + 35 + 70	w/o

seismic response of the case-study prototypes. Accordingly, upper and lower bounds were provided for capacity estimations of such reinforced precast concrete wall systems, assuming values of axial load that are comparable to those applied in practice. Even and odd specimen labels identify the maximum and minimum axial load imposed during the test, namely  $N_{max}$  and  $N_{min}$ , which correspond to axial load ratios ranging approximately from 3 to 1%. Regardless of the window or door configuration herein denoted as W and D, specimens presenting a cutout in their layout were tested assuming 360 and 140 kN as maximum and minimum initial axial load level.

In accordance with Dutch construction practice for such structures, starter rebars protruding from the foundation were considered or not depending on the wall thickness. In addition to longitudinal and transverse reinforcement, two 500 mm long starter rebars were indeed provided at the corners of specimen 01. By contrast, this type of detailing was omitted in the other panels, which were directly set in place by seating them onto the foundation. As shown in Fig. 3a, Ø100 channels were embedded at 300 mm from both panel corners, permitting the steel dowels to be set in place. After their anchorage into precast members, these hollow profiles were grouted up to approximately a quarter of wall height, taking advantage of the same concrete mix used in the panel construction.

Minimum reinforcement requirements prescribed by current European rules (CEN, European Committee for Standardization 2004a; Nederlands Normalisatie-instituut 2011) were imposed for each specimen under investigation. As depicted in Fig. 4, additional rebars were provided at the corner of the opening, in case of specimens presenting a window or a door. As such, the spacing of longitudinal reinforcement was slightly adjusted in these cases in order to comply with the updated geometries, resulting in an almost negligible difference for what concerns the volumetric reinforcement ratio of these prototypes. Steel type B450C was used for both longitudinal and transverse reinforcement, while concrete class C35/45 according to Eurocode 2 (CEN, European Committee for Standardization 2004a) was used for all specimens under consideration, as mentioned in Sect. 2. Compressive tests were performed on  $150 \times 150 \times 150$  mm concrete cubes at 28 days, showing strengths higher than those specified by code provisions (i.e. 13%). The mean 28-day compressive strength was 49.4 MPa, compared to a mean code-compliant threshold of 43 MPa. Similarly, tensile strengths higher than those specified by the supplier can be observed for reinforcing steel in accordance with the characterization tests carried out.

As shown in Figs. 3 and 4,  $200 \times 150$  mm niches were settled in correspondence to the inner edge of each wall segment in order to arrange the top and bottom panel-to-panel

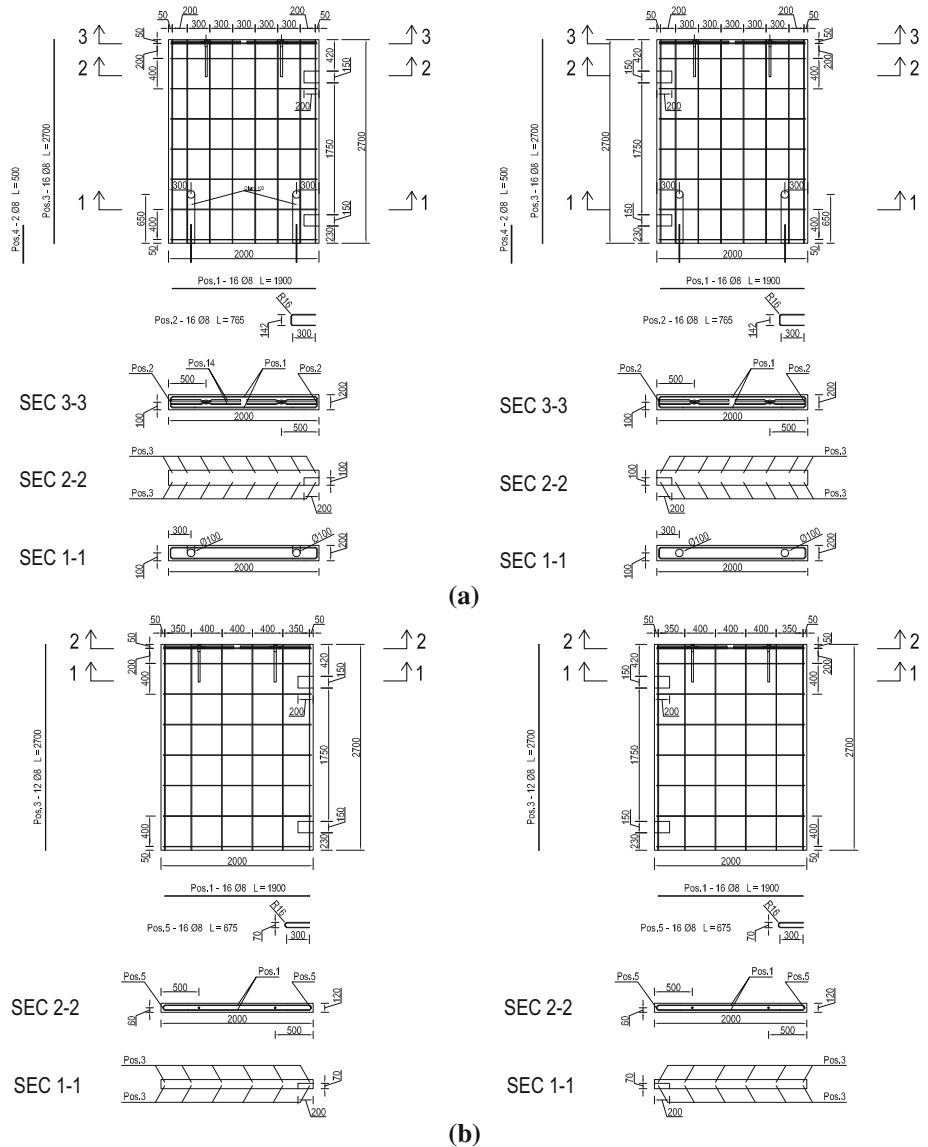


**Fig. 3** Details and reinforcement layout of prototype wall systems with and without starter rebars: **a** specimen 01; **b** specimen 02

connections consisting of threaded M8 anchors made of steel grade 8.8. Figure 5 presents a sketch of mechanical connectors and anchoring system composed of threaded bolts and steel plates, which were used to fasten the hook reinforcement to the external longitudinal rebar of each panel segment. A representative example of the execution of these joints is provided in Fig. 5 as well. After their arrangement into the niches, a low-strength mortar with a compressive resistance at 28 days equal to 15 MPa was selected for the injection grout. The same type of hooked anchor rod was used for different typologies of precast



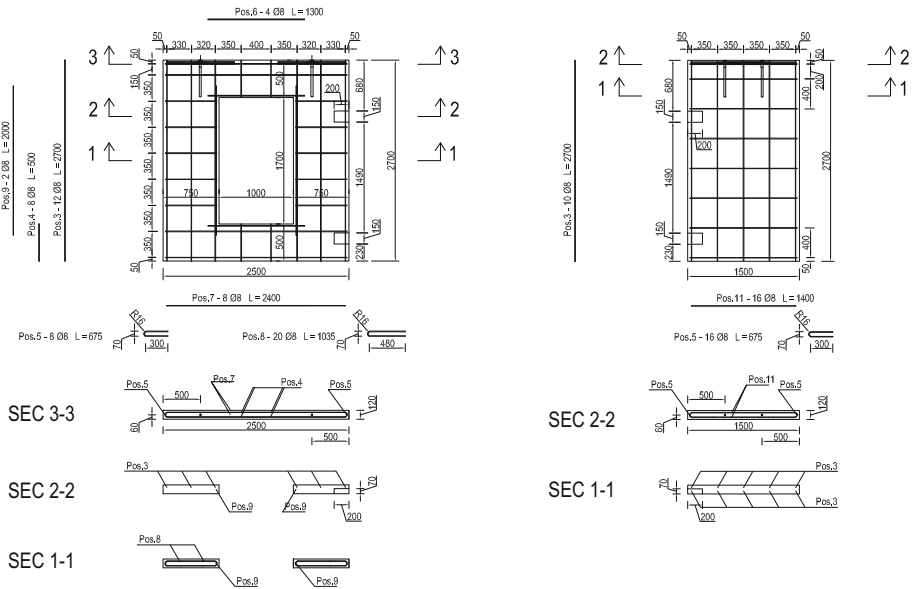


**Fig. 4** Details and reinforcement layout of prototype walls with an opening—specimen 04

panels and their embedment depth into the wall was assumed to be approximately equal to 100 and 70 mm for 200 and 120 mm thick specimens, respectively. The anchoring zone was arranged at 680 and 230 mm from the top and bottom of each wall system presenting an opening (see Fig. 4). By contrast, the position of top wall-to-wall connections was slightly uplifted (i.e. 420 mm) in case of specimens without a window or a door (Fig. 3), as commonly done in Dutch practice.

More specific details concerning the rationale behind the design of the experimental setup in terms of boundary conditions (i.e. concrete foundation, top steel beams and sliding restrainers) and application of vertical and horizontal loads (i.e. hydraulic jacks and actuators) are discussed in the following section.

### 3.2 Test setup and loading protocol

The series of full-scale panels were subjected to a combination of horizontal and vertical loading, assuming a single bending loading scheme for each one of them. A quasi-static cyclic displacement history at progressively increasing interstorey drifts was imposed by a MTS actuator in displacement control. In particular, the experimental loading protocol consisted of a set of eight symmetric horizontal drift targets:  $\pm 0.1$ ,  $\pm 0.2$ ,  $\pm 0.4$ ,  $\pm 0.6$ ,  $\pm 0.8$ ,  $\pm 1.0$ ,  $\pm 1.2$ , and  $\pm 1.5\%$ . It is worthwhile to mention that drift was defined as the difference between the displacements at the top and bottom of the panel normalized by the height of the panel itself. As reported in Table 2, three cycles per amplitude were planned. In addition to the aforementioned drift levels, two series of cycles were initially applied in force control (see Table 2). The loading rate was in the range 0.045–0.675 mm/s, the higher rate corresponding to higher displacement amplitude. Hydraulic jacks, acting on the top steel beams and connected to the concrete foundation at the base of the panels, were used to apply the constant axial load (Table 1). In case of cantilever walls without openings, the axial load was exerted by a set of two hydraulic cylinders with automated

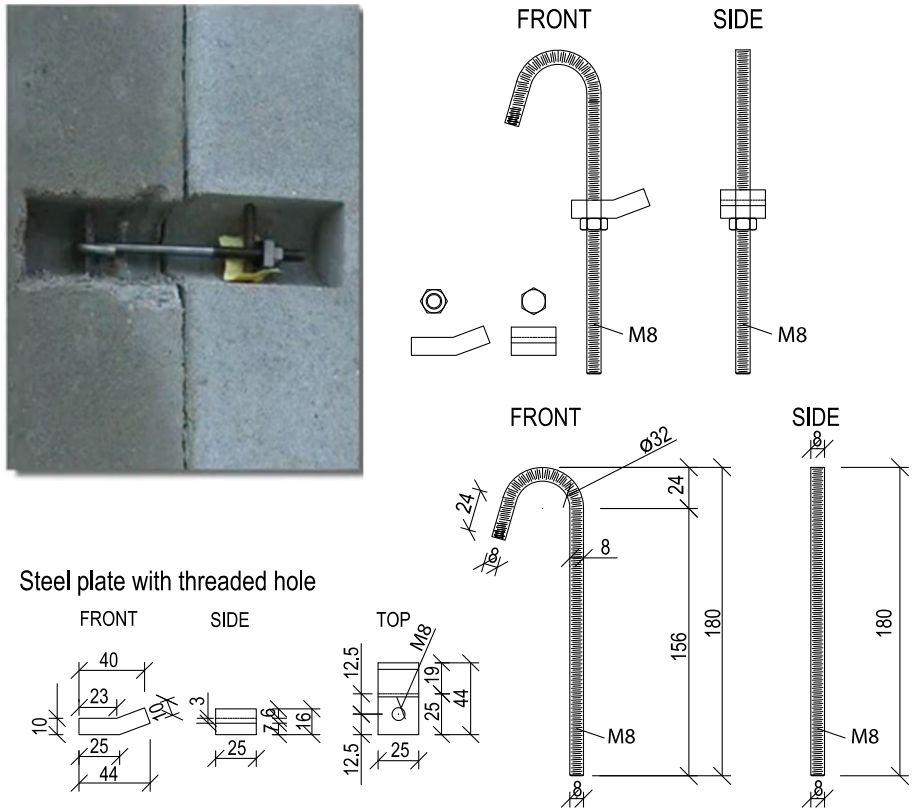


**Fig. 5** Representative example of anchoring system for wall-to-wall connections: schematics of steel plates and threaded M8 anchors. Note front and side views

pressure self-adjustment, acting against four vertical rods that were connected to the strong floor of the laboratory through hinges (see Fig. 6a). By contrast, four jacks (instead of two) were post-tensioned to the concrete footing, when testing panels with an opening, in accordance with the experimental setup shown in Fig. 6b. It can be noticed that two of those hydraulic cylinders were symmetrically arranged at the top of the 1.5 m long wall segment in order to apply the axial load along its vertical axis (Fig. 7b).

In addition to the test setup, Fig. 6 schematically presents typical panel instrumentation, which was used to measure absolute and relative quantities at key locations throughout each type of specimen. According to wall geometry, a series of potentiometers were arranged to monitor displacements at different levels along the height of the panel, its flexural and shear deformations, base uplift and slippage in the concrete footing. To prevent/minimize any type of undesirable local mechanism, particular care was paid to the definition of the test setup and, hence, a series of high-definition solid finite element (FE) models based on classical principles of nonlinear fracture mechanics (Brunesi et al. 2015b; De Borst 1987; Hung and El-Tawil 2010) were developed to study the influence of different design assumptions on the structural response of the case-study specimens.

Considering that the experimental program focused mainly on wall-to-wall connections, a flanged 10 mm thick clip angle was provided in correspondence to the top and bottom

**Table 2** Example of experimental loading protocol (force and displacement control mode)—specimen 01

Test #	Test name	Main DoF	Control type (force or displ.)	MAX ampl. (kN mm)	MIN ampl. (kN mm)	Loading speed (kN/s mm/s)	Load shape	Axial load (kN)	Cycles (#)
0	Axial	Vert.	Force	0	−400	3.333	Ramp	—	—
1	Drift #01	Long.	Force	50	−50	0.833	Triang.	400	3
2	Drift #02	Long.	Force	100	−100	1.667	Triang.	400	3
3	Drift #03	Long.	Displ.	2.7	−2.7	0.045	Triang.	400	3
4	Drift #04	Long.	Displ.	5.4	−5.4	0.090	Triang.	400	3
5	Drift #05	Long.	Displ.	10.8	−10.8	0.180	Triang.	400	3
6	Drift #06	Long.	Displ.	16.2	−16.2	0.270	Triang.	400	3
7	Drift #07	Long.	Displ.	21.6	−21.6	0.360	Triang.	400	3
8	Drift #08	Long.	Displ.	27	−27	0.450	Triang.	400	3
9	Drift #09	Long.	Displ.	32.4	−32.4	0.540	Triang.	400	3
10	Drift #10	Long.	Displ.	40.5	−40.5	0.675	Triang.	400	3

corners of each panel assembly, in order to minimize/inhibit sliding mechanisms from taking place at the concrete foundation-precast wall interface. In particular, these sliding restrainers consisted of a 300 × 200 mm L-shaped steel plate screwed and bolted to the bottom concrete and top steel beams by means of four threaded M20 anchors. Such a system was additionally strengthened through a 10 mm thick 200 mm deep welded flange. Although such stoppers are not used in practice, a similar level of constraint can be ensured by other adjacent panels, which are present in real/actual buildings. It was thus decided to take advantage of the aforementioned restrainers in order to avoid damage in the setup or instrumentation and to be as representative as possible of this type of boundary conditions.

For application and distribution of vertical and horizontal loads, HE300A steel profiles stiffened by 10 mm thick plates welded at 150–250 mm spacing were screwed to the top of each specimen (see Fig. 7). The top steel beams designed to remain in their elastic regime were split in two segments, and a 5 mm thick layer of Teflon (PTFE) was provided to inhibit/minimize the frictional force transfer at beam–beam interface. Accordingly, this approach was planned to simultaneously permit (1) the transfer of horizontal load imposed by the MTS actuator, and (2) the release of relative motion among wall segments in vertical direction (i.e. rocking/sliding). Nevertheless, it is worth noting that, in some cases, the two top beams were observed to come in contact at their edges for large levels of imposed horizontal drift (>1%). As a result of this undesirable mechanism, spurious resistance overestimates were sometimes measured at the last cycles of the testing protocol, as discussed in the following section.

### 3.3 Experimental results and observations

In the framework of this experimental investigation, failure of the tested specimens was identified according to three performance criteria that were distinctly defined either at global or local levels:

1. First exceedance of a conventionally fixed drift limit (i.e. 1.5%);
2. First attainment of a conventionally fixed decrease in load bearing capacity (i.e. 20%);

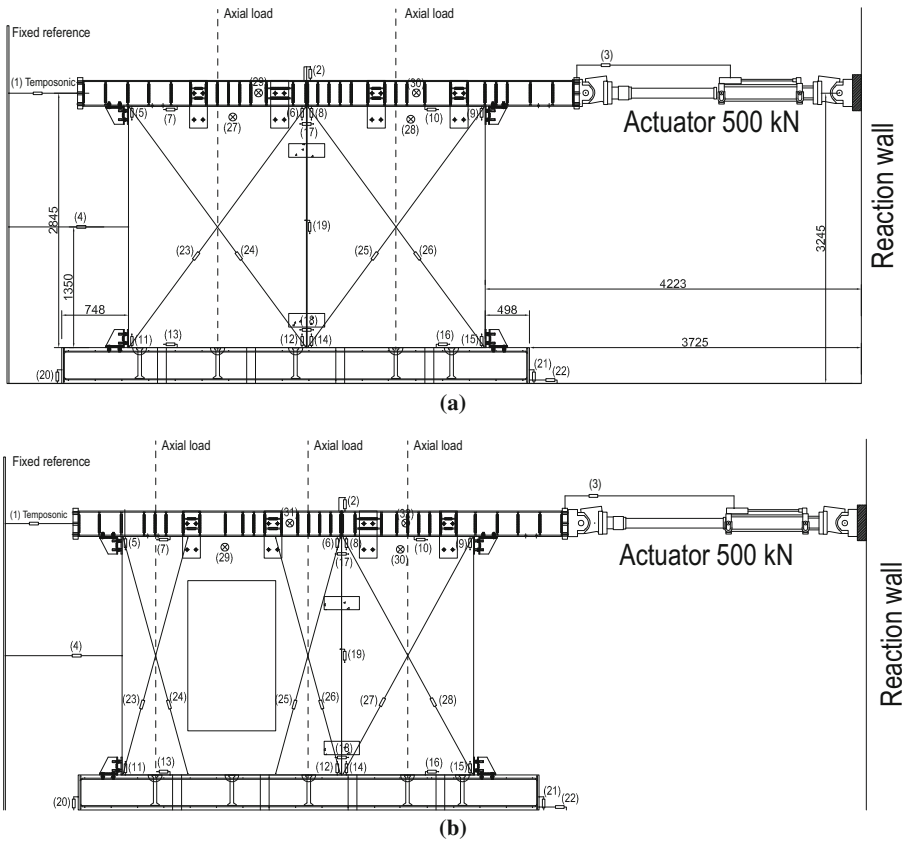


**Fig. 6** Schematics of test setup and instrumentation for panels (a) without an opening—specimens 01, 02 and 03; (b) with a window—specimens 04 and 05

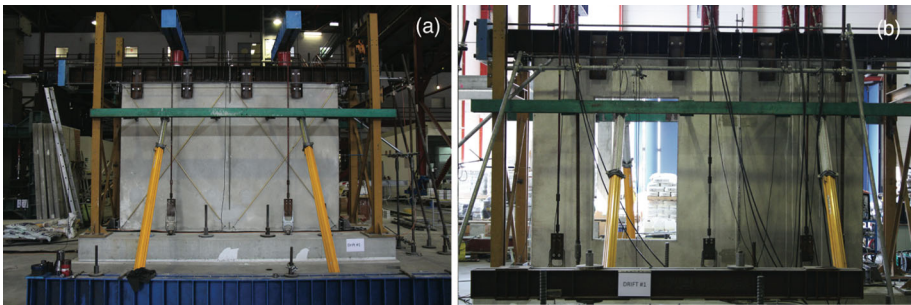


**Fig. 7** Photographs of panels tested in single bending configuration—loading scheme and top steel beams: a specimen 01; b specimen 04

3. First shear-buckling fracture of a mechanical connector in the panel-to-panel joints.

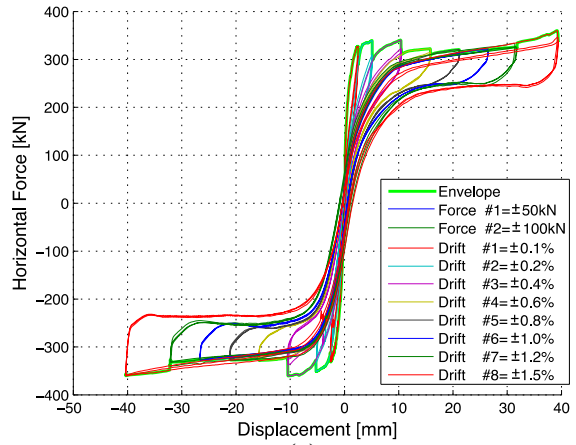
The first occurrence of one of the three ultimate conditions listed above was thus interpreted as a conservative check of the “near collapse” limit state for the panel

prototypes under consideration. As expected, all the tested specimens were observed to collapse by the premature shear failure of their connections because of kinematics that attracted unintended forces in poorly detailed joints, primarily constituted by steel dowels and mostly relying on shear friction for the horizontal load transfer between structural members. Therefore, the intrinsic lack of shear and ductility capacity shown by this type of connection system results in a local failure, which in turn implies a global-structural collapse of the tested panel assemblies. These aspects are crucial considerations that can be drawn towards the improvement of their early design, as precast walls may nowadays emulate the response of a cast-in-place construction with lapped reinforcing bars in concreted/grouted joints, or alternatively they may be designed with discrete joints that are capable of dissipating energy through ductile connections or damping devices. Thus, connections can be either (1) strengthened to ensure that the relative displacements/rotations between adjoining wall segments are minimized or (2) rationally conceived to properly allow for displacement demand rather than to attempt strain and load levels that might be unfeasible, depending on the design target of each specific case-study.

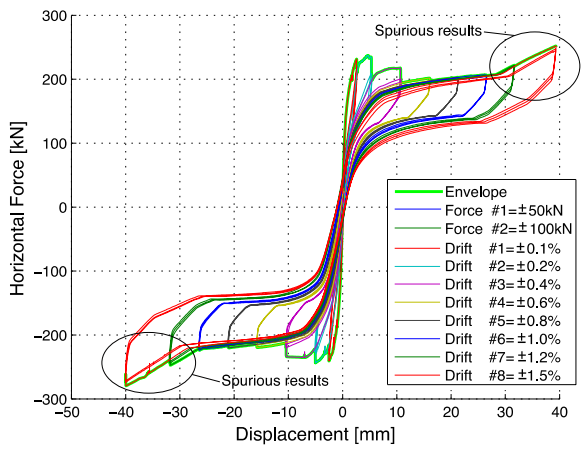
Figure 8 shows the cyclic response of the three cantilever wall systems without openings in terms of horizontal force–displacement capacity curves; in particular, Fig. 8a presents the hysteresis loops obtained for the 200 mm thick panel tested. Considering the first cycle of each drift amplitude, specimen 01 resisted a maximum lateral load of 331, 351, 360, 328, 327, 328, 340, and 361 kN at top horizontal displacements of up to 2.5, 5.2, 10.4, 15.8, 21.1, 26.6, 32.1, and 40.3 mm, respectively. Experimental predictions revealed an almost symmetric response during pulling and pushing phases, either in terms of forces or displacements, as only a slight discrepancy of up to 4% was observed because of the combined effects of damage and slippage in the components of the connections. After minor cracking, incipient yielding occurred at drift levels roughly equal to 0.15% for an actuator load of approximately 340 kN, while the peak capacity of prototype 01 (i.e. 360 kN) was recorded for a slightly higher drift level equal to 0.2%. As drift demand was increased, the response was mostly characterized by rocking mechanisms that resulted in panel uplift at its base and shear failure of its top and bottom wall-to-wall connection systems. A gap opened up on the bottom edge of the wall but closed on the top edge due to the presence of the adjoining panel. During the cyclic reversal, the opposite wall segment reseated itself and then began to bear on the other, resulting in an additional demand at the level of the connections, which were observed to be the most damaged zones of the structural system tested (see Fig. 9). When incipient rocking took place (i.e. drift target #05), the peak capacity decreased approximately by 10%—compared to maximum horizontal load—and remained fairly constant for larger drift amplitudes. The slight increase of lateral bearing capacity caused by the application of 1.5% drift cycles was mainly ascribed to the test setup, as previously mentioned. More in detail, the rocking mechanism of adjacent panels induced a rotation of the actuator loading line, and hence, the applied force measured by the load cell had a vertical component resulting in a fictitious increment of horizontal capacity. Equilibrium and compatibility equations, together with the kinematics measured during the test, were used to quantify analytically such increment, which was nonetheless found to be relatively moderate (i.e. 5%, at 1.5% drift). Noteworthy is that this conclusion was also supported by the proposed numerical model (see Sect. 5), as it is refrained from having components other than the imposed horizontal one (i.e. non-follower forces) and thus can be referred to as a reliable reference for the evaluation of this effect.

Figures 10 and 11 collect the primary damage mechanisms of 120 mm thick wall systems in case of maximum and minimum axial loads, while their lateral force versus displacement curves are reported in Fig. 8b, c respectively. In the latter case, the

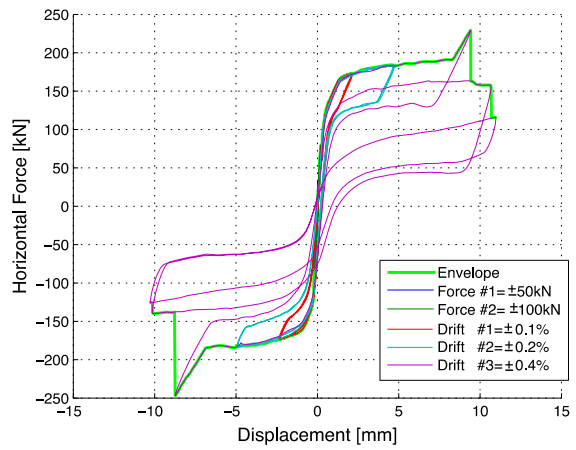
**Fig. 8** Horizontal force–displacement curves of wall systems without opening: **a** specimen 01; **b** specimen 02; **c** specimen 03



(a)



(b)



(c)

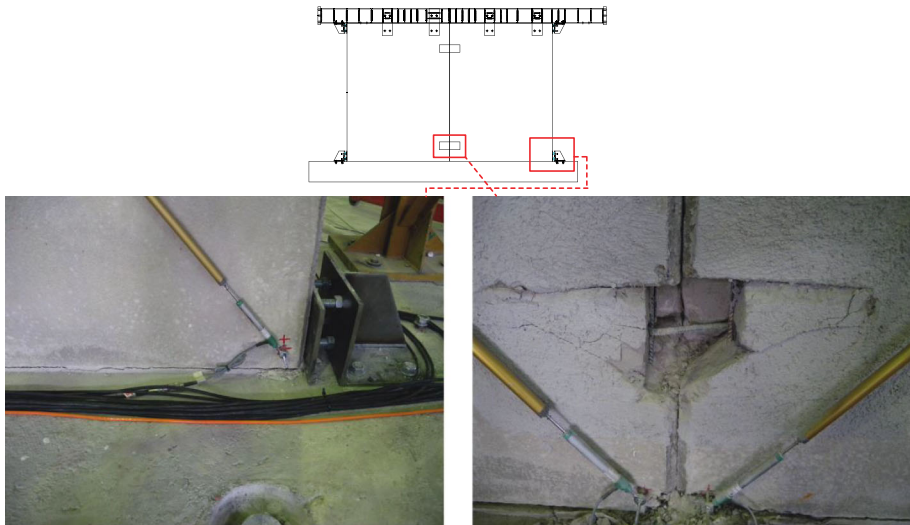


**Fig. 9** Damage mechanism of specimen 01: crack induced by panel uplift and rocking at the base (*left*); failure of wall-to-wall connection system (*right*)

application of horizontal drifts slightly smaller than 0.4% was observed to cause a premature connection failure that resulted in a pronounced out-of-plane misalignment between the two panels of specimen 03. An example of this local/global collapse mode is provided in Fig. 11. In addition, Fig. 10 confirms that buckling/shear failure of steel dowels in combination with a moderate concrete spalling/crushing at the base of the wall play a key role in the cyclic response of such structural systems. The hysteretic behavior of specimen 02 (see Fig. 8b) was primarily governed by rocking and, even in this case, the load picking up recorded in the last steps of this test—corresponding to a drift amplitude of 1.5%—was attributable to the experimental setup (Fig. 10). A direct comparison between specimens 02 and 01 (Fig. 8b vs. Fig. 8a) also reveals that 120 and 200 mm thick prototypes present hysteresis loops similar in shape and character but different in terms of load carrying capacity, as a consequence of a different axial force imposed (i.e. 500 vs. 800 kN). In detail, specimen 02 resisted peak horizontal loads approximately 30–40% lower than those shown by specimen 01 for the same level of lateral drifts. Furthermore, Fig. 12 presents the lateral stiffness decrease that was observed for these two specimens, thus confirming that prototypes with and without starter rebars are characterized by similar trends. In turn, this implies that the presence of such starter bars, which were designed and arranged to protrude less than 200 mm into the panels, has a relatively moderate influence on the response of this type of wall system, mainly because of their development length. Noteworthy is that, although a solution like this is in contrast with common earthquake engineering practice, it was found to be very common for these precast houses in the Netherlands and the same applies to the use of smooth starter rebars. For the sake of clarity, one may note that the comparison shown in Fig. 12 refers to panel assemblies with different wall thicknesses because the starter rebars are present or not depending on this parameter. Therefore, the values of secant stiffness obtained for increasing drift amplitudes by the hysteretic curves of specimen 01 (with starters) and specimen 02 (without starters) were normalized with respect to the secant stiffness determined for each specimen at 0.1% drift. The first of the three cycles performed for each drift amplitude was taken as

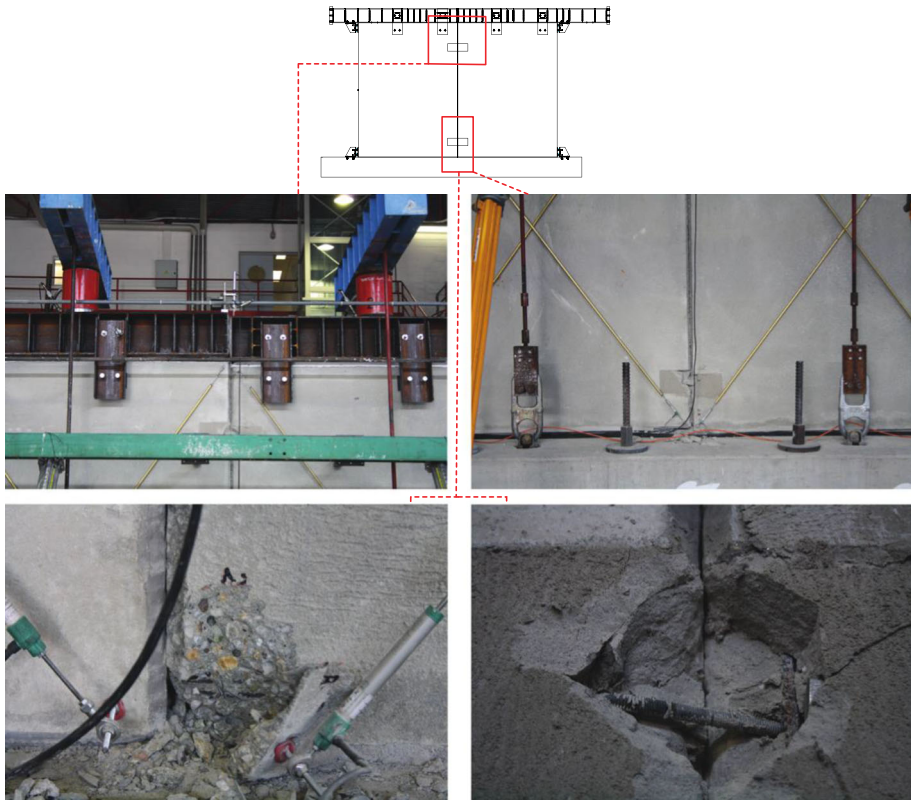


**Fig. 10** Damage mode of specimen 02: rocking mechanism and relative vertical displacement between wall segments—detail at the top and bottom of the assembly (*top left* and *top right*); concrete spalling at the base of panel assembly (*bottom left*); example of buckling of the anchor rods in wall-to-wall joints (*bottom right*)

reference, even though similar considerations can be drawn from the second and third cycles as well.

The cyclic load–displacement response of cantilevered wall systems presenting an opening in their structural layout are provided in Fig. 13, showing different behavioral aspects in case of specimens with a window (i.e. Fig 13a, b) or a door (i.e. Fig 13c, d). Nevertheless, asymmetric capacity curves can be observed during pulling and pushing phases in both cases because of the asymmetric geometry of panel segments. A discrepancy of up to 20% was predicted for specimens 04 and 05, while an even higher mismatch in the range 30–50% can be highlighted for prototypes having a door. Regardless of the axial load imposed, the former prototypes reveal pronounced hysteresis loops, whose envelope is characterized by a significant hardening in the post-yielding regime of the response. Under minimum axial load level (i.e.  $N_{min}$ —specimen 05), incipient yielding took place at 0.2% drift cycles for an actuator load of about 140 kN, while the peak capacity of prototype 05 was observed for the last drift amplitude imposed (i.e. 1.2%), thus confirming that no lateral strength degradation occurred during the test due to the propagation of diagonal cracks at the corners of the window. A similar response was obtained for a higher axial load (i.e.  $N_{max}$ —specimen 04), as also in this case the horizontal force increased for increasing drift amplitudes without any type of strength degradation.



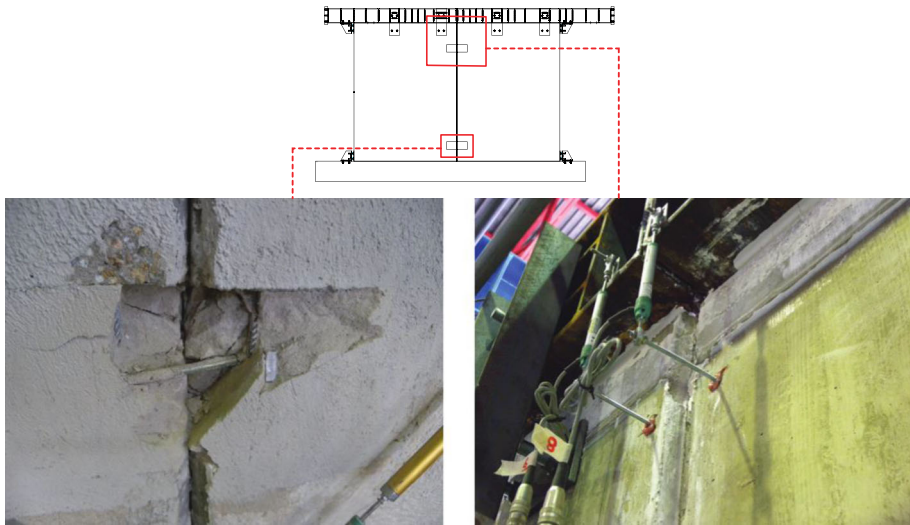
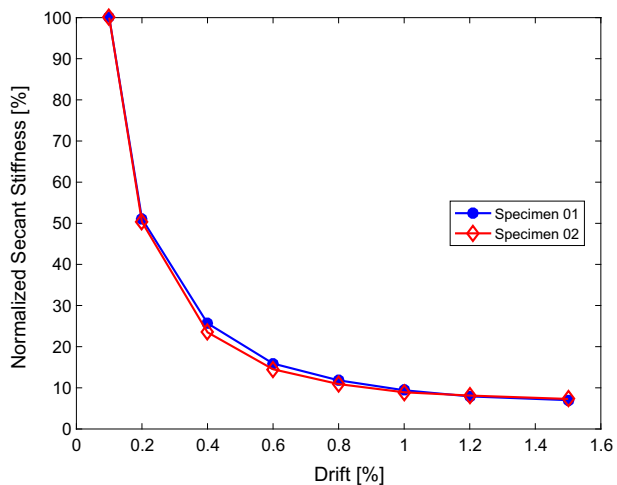


**Fig. 11** Damage mechanisms of specimen 03: premature connection failure in the *bottom wall-to-wall joint* (left); out-of-plane misalignment between the two panels at the end of the test (right)

**Fig. 12** Normalized secant stiffness versus drift relationship for specimens with and without starter rebars



Backbone curves without softening behavior were also shown by other experimental programs on walls with openings [see e.g. (Pavese and Bournas 2011; Todut et al. 2014)]. As shown in Figs. 14 and 15, where the damage patterns of specimen 04 and 05 are collected, those two panel assemblies were also characterized by collapse mechanisms in close agreement with each other. In both cases, diagonal cracks formed at 0.2% drift cycles in correspondence to the four corners of the window. As the imposed lateral deformation was increased, they developed and propagated up to failure, confirming that a resisting mechanism other than that observed for walls without openings took place in this case. Concrete cracking and crushing was more significant in the case of specimen 05 and resulted in visible buckling of the longitudinal rebars at the bottom left and right corners of

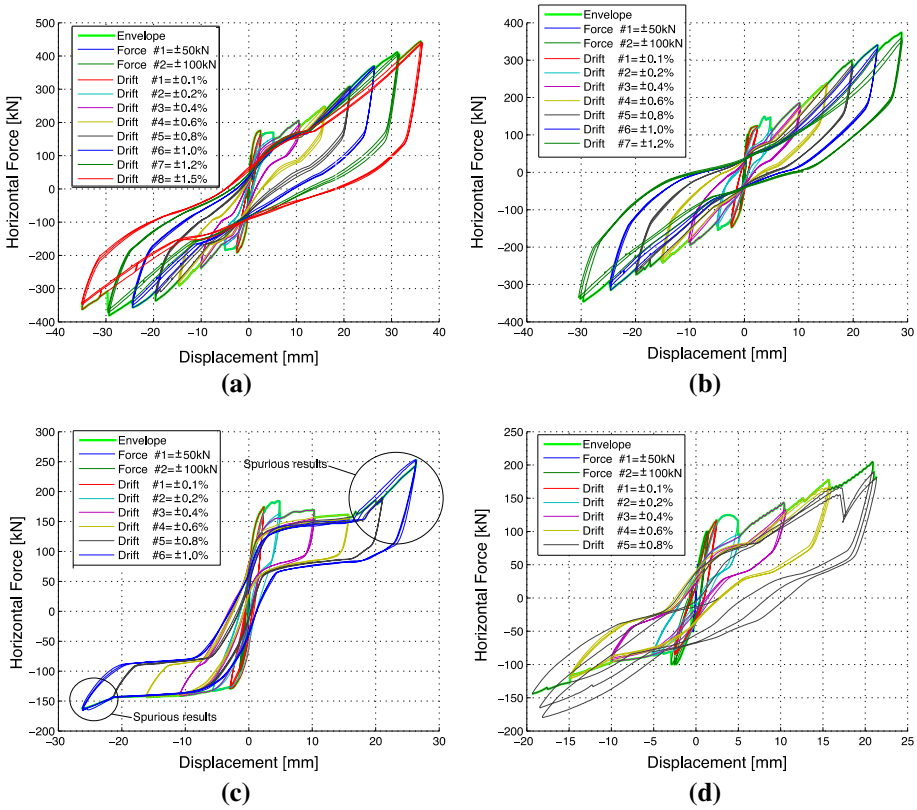


**Fig. 13** Horizontal force–displacement curves of wall systems with an opening: **a** specimen 04; **b** specimen 05; **c** specimen 06; **d** specimen 07

the window, in combination with a simultaneous shear failure of anchor rods in the wall-to-wall joints (see Fig. 14). However, it can be noticed that the crack patterns shown in Figs. 14 and 15 refer to two different levels of imposed lateral deformation, as in the latter case the test was interrupted at 1.0% (instead of 1.2%) drift amplitude. In both cases, this mechanism was associated with gradual stiffness degradation and stable hysteresis loops characterized by equivalent viscous damping in the range 11–17%, the lower value corresponding to higher displacement amplitude. In terms of secant stiffness, a visible decay occurred after the yielding condition was exceeded (i.e. 54 and 36% if the first 0.2 and 0.4% drift cycles are considered, respectively) but values in the range 8–17% were determined at larger drift amplitudes. A moderate decrease was observed as the number of constant amplitude cycles at a given drift level increased. Considering the first and second cycles, the maximum decay (8%) was obtained at 0.2% drift and the minimum (2%) at 1.5% drift. The equivalent viscous damping, which was computed by equating the area enclosed by a complete hysteresis loop and the energy absorbed by the hysteretic steady-state cyclic response at a given displacement level, presented similar trends, as this parameter was observed to decrease as the imposed drift level increased or alternatively as the number of constant amplitude cycles for a constant drift level increased, particularly between the first and second cycles. In both cases, the maximum decay was determined

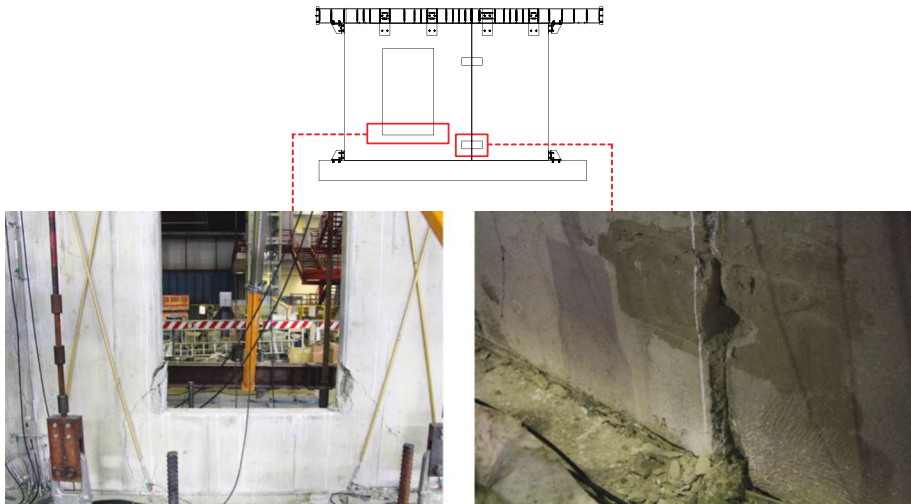


**Fig. 14** Crack pattern and failure mode of specimen 04: concrete crushing at the corners of the window and buckling of longitudinal reinforcing rebars (*left*); out-of-plane misalignment and failure of the anchors (*right*)

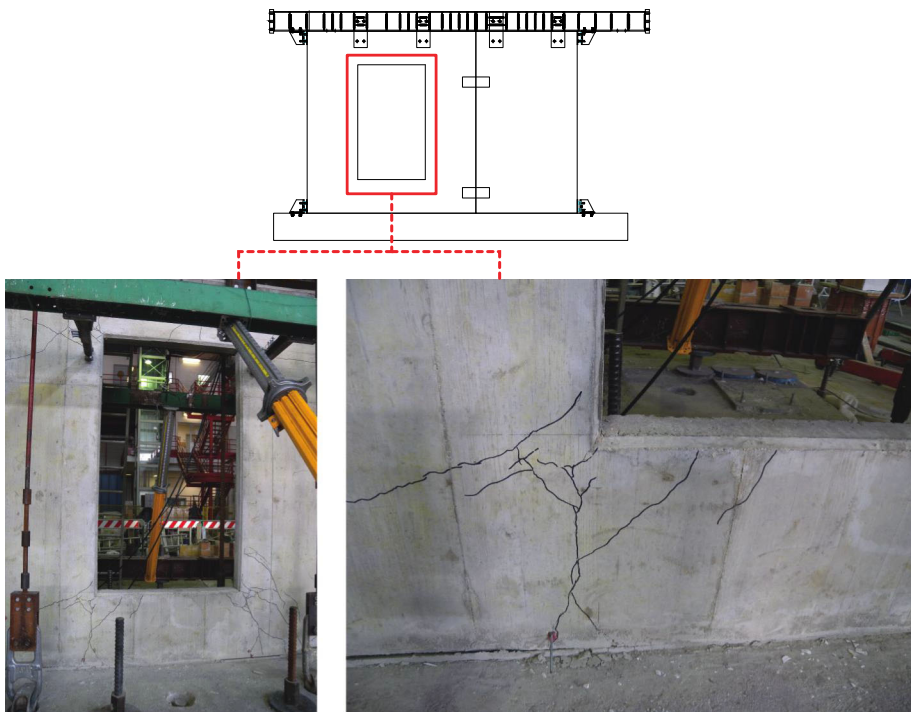


**Fig. 15** Crack pattern and failure mode of specimen 05: propagation of diagonal cracks at the corners of the window (*left*); detail of the bottom left side corner (*right*)

after the exceedance of the yielding condition and corresponds approximately to 24 and 13%, respectively.

A more complex response was obtained in case of specimens 06 and 07, as evidenced by their horizontal force–displacement curves (see Fig. 13c, d) and inherent damage mechanisms (Figs. 16, 17). In both wall systems, the classical base uplift resulting from rocking behavior of the prototypes was associated with the formation and propagation of a pronounced horizontal crack at the right corner of the door. In addition, the shear/buckling collapse mode of panel-to-panel anchors caused a visible detaching of the two wall segments for each specimen under consideration. Concrete spalling/crushing at the base of the panel was also observed for specimen 07, while pounding during cyclic loading reversals was slightly more significant in case of specimen 06. Despite similar failure modes, hysteresis loops slightly different in character can be observed for specimen 06 and 07 because of the different axial load levels applied during the test. Under maximum axial force level (i.e.  $N_{max}$ —specimen 06), the cyclic load–displacement response was primarily controlled by rocking in the small-medium displacement range (i.e. 0.2–0.6% drift cycles). The mechanism was stable and the load carrying capacity remained fairly constant at

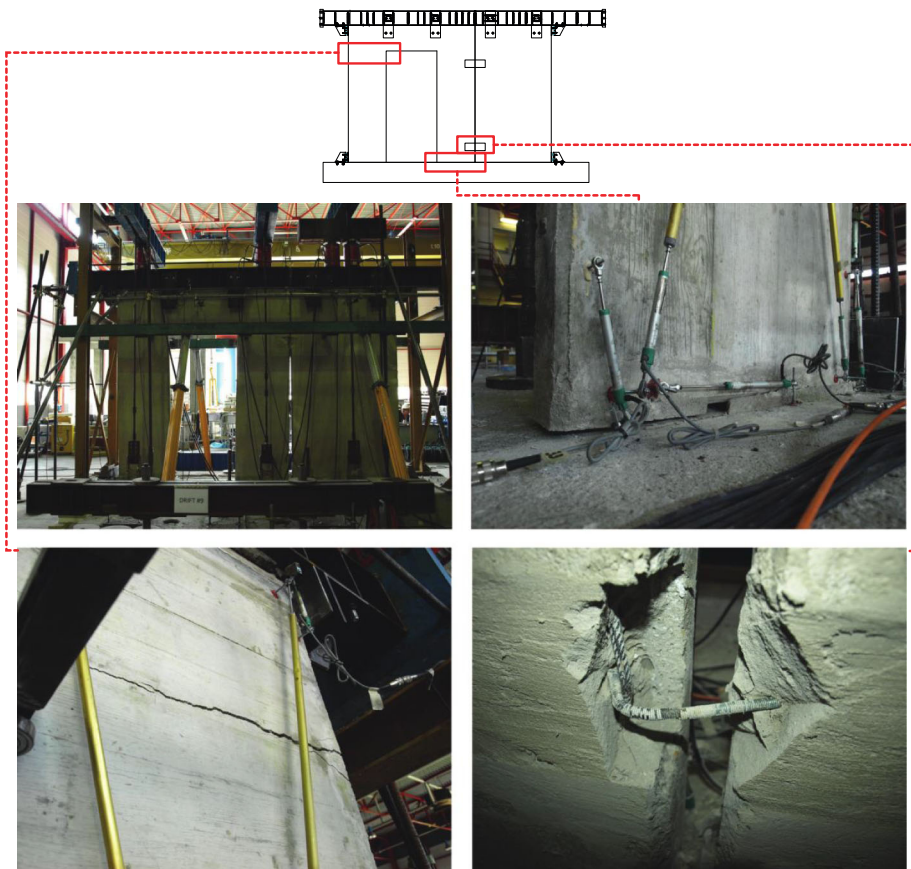


**Fig. 16** Damage mechanism of specimen 06: deformed shape at the end of the test and detaching of the two panels (*top left*); rocking and base uplift (*top right*); propagation of horizontal cracks at the corner of the door (*bottom left*); failure of the anchors—detail of the bottom wall-to-wall connection (*bottom right*)



**Fig. 17** Damage mechanism of specimen 07: deformed shape at the end of the test—detaching and pounding between wall segments (*top left*); failure of wall-to-wall connection systems (*top right*); concrete spalling and crushing at the base of the wall (*bottom left*); concrete crushing and buckling of longitudinal rebars at the corner of the door (*bottom right*)

increasing drift demands. By contrast, the application of minimum axial load (i.e.  $N_{min}$ —specimen 07) caused a more significant interaction between geometric and material sources of nonlinearity (i.e. rocking and plasticity), thus implying an increase of horizontal force at increasing lateral displacements. Hysteresis loops weakened in character can be observed at 0.8% drift cycles as a consequence of prominent concrete crushing at the top right corner of the door, which was combined with a visible buckling mode of the longitudinal rebars (see Fig. 17).

The set of lateral force-drift curves obtained for prototypes with the same geometry but different levels of imposed axial loads are compared in Fig. 18, while Fig. 19 systematically quantifies the influence of degradation on the seismic response of a reference wall system tested (specimen 01). Considering 120 mm thick panels, specimen 02 resisted peak horizontal loads 25–28% higher than those obtained for specimen 03 at the same level of lateral drifts. As highlighted in Fig. 18a, the evaluation of behavioral changes is limited to the small displacement range because of the premature global collapse of specimen 03 at 0.4% drift cycles. In this range, similar effects/trends can be observed in case of specimens

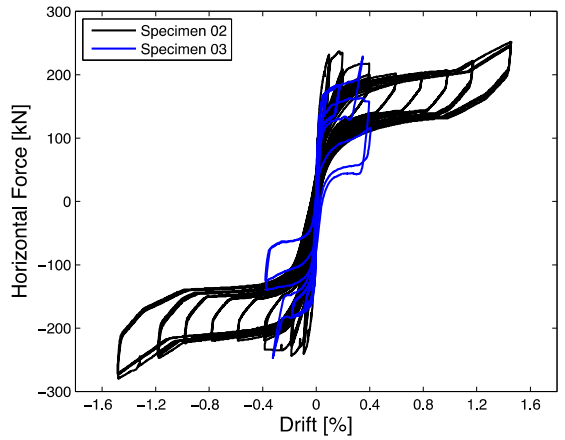
having an opening in their layout, as shown in Fig. 18b, c. A discrepancy in the range 25–29% was indeed determined by comparing specimen 04 and 05, and the comparison between specimens 06 and 07 resulted in a similar mismatch of 27–30%. Different considerations can be drawn at larger drift amplitudes, as in both cases a difference of about 10% can be computed in terms of peak horizontal force. Thus, it can be noticed that a variation in the imposed axial load causes a difference of about 25–30% in the small displacement range, regardless of the presence of an opening. The comparison between walls with a window (i.e. specimen 04 vs. 05) and walls with a door (i.e. specimen 06 vs. 07) leads to similar results, regardless of the drift range considered. A similar difference was indeed observed for the small drift range (i.e. approximately 25–30%) and for larger drift levels (i.e. roughly 10%).

The sensitivity of response degradation to the number of constant amplitude cycles at a given drift level was presented in Fig. 19, where the effects produced by an increase in the drift level imposed were provided as well. Comparisons were systematically derived and shown in terms of (1) force-drift response, (2) secant stiffness, (3) peak strength, and (4) dissipated energy for a specific case-study panel assembly. Narrow thin-shaped hysteresis loops with moderate and gradual strength degradation can be observed for specimen 01 after the yielding condition was exceeded (see Fig. 19a). As also highlighted in Fig. 19c, fairly constant horizontal peak forces were indeed obtained after the activation of rocking mechanism. As expected, this type of response was associated with moderate energy dissipation capacity and gradual stiffness deterioration. In this case, the maximum decay (48%) was observed at 0.2% drift and the minimum (12%) at 1.5% drift. As presented in Fig. 19b, an almost negligible degradation (<10%) can be shown between the first and second cycles, and a similar consideration can be drawn for the second and third cycles. Low equivalent viscous damping ratios can be computed from the set of energy dissipation estimates collected in Fig. 19d, as values of up to 10% were determined in the small displacement range. Values even lower (i.e. 6–7%) were observed at larger drift levels, thus confirming estimates close to those attained in case of a pseudoelastic response.

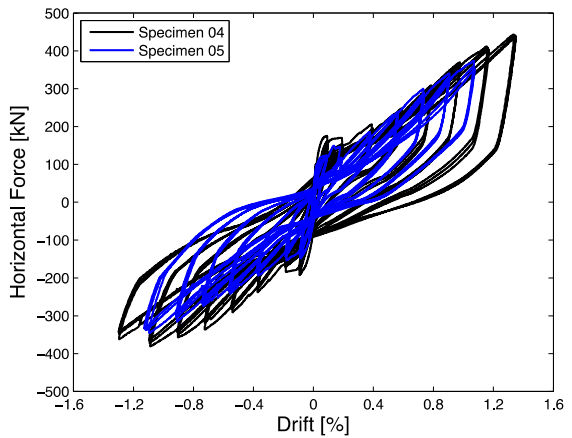
#### 4 Asymmetric push–pull tests of precast connection systems

The second phase of the experimental investigation carried out and reported herein was chiefly concerned with experimental testing of precast connections aimed to provide a clear understanding on their seismic behavior and, hence, data valuable for modeling such types of dry joint systems that are commonly used in Dutch construction practice for prefabricated lightly reinforced concrete walls. To this aim, four additional specimens were constructed and assembled, and a series of displacement-controlled asymmetric push–pull tests were performed, as specified later on in more details. The following sections present a brief description of geometrical characteristics, material properties and reinforcement layouts of those panel subsystems, as well as a summary regarding the experimental setup and loading protocol assumed for this complementary set of tests. Finally, capacity curves and damage mechanisms obtained from the experimental activity were collected and discussed to examine peculiar behavioral aspects for such a common form of connection system in precast buildings of the Dutch market.

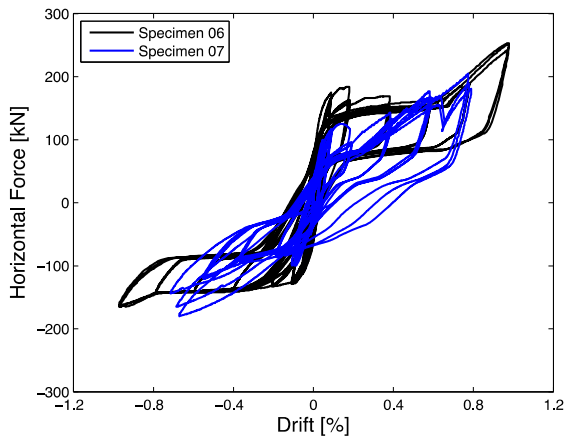
**Fig. 18** Influence of axial load—comparison between hysteretic response of tested prototypes: **a** specimen 02 versus 03; **b** specimen 04 versus 05; **c** specimen 06 versus 07



(a)



(b)



(c)

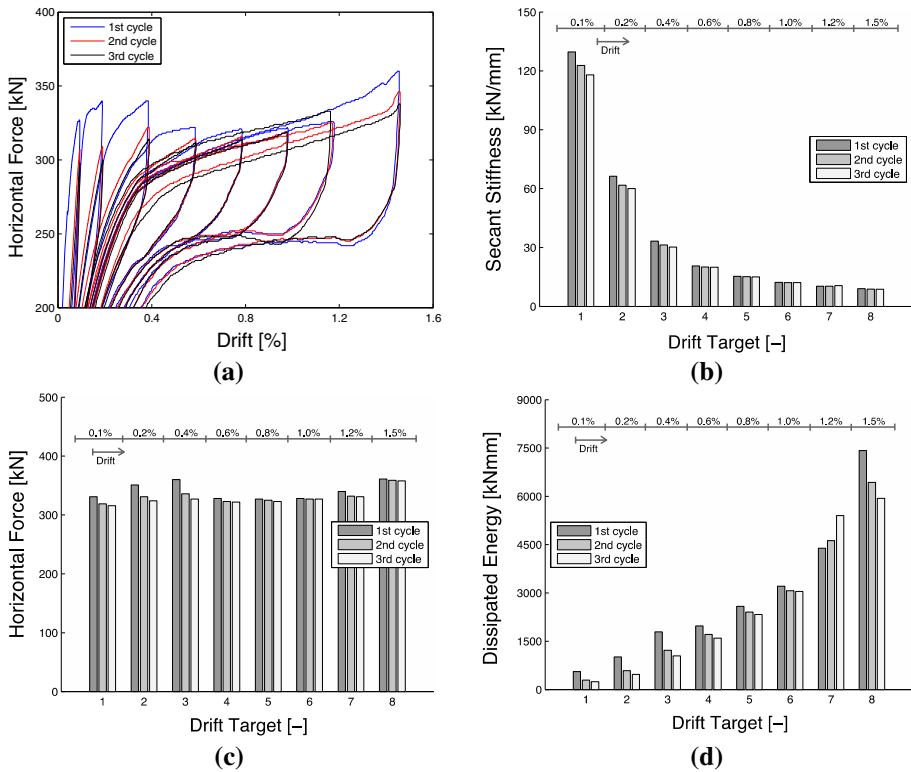


**Fig. 19** Effects of degradation with the number of cycles – specimen 01: **a** force-drift response; **b** secant stiffness; **c** peak resistance; **d** dissipated energy

### 4.1 Description of precast subassemblies

Table 3 provides the experimental parameters, along with the specimen nomenclature used in the upcoming discussion of test results. Each prototype consisted of two 1 m long, 2 m wide precast panels that were assembled as shown in Fig. 20, where an example of reinforcement layout is also given. Two values of thickness (i.e. 120 and 200 mm) were assumed in accordance with those considered for cyclic tests on full-scale wall systems (see Sect. 3.1) and, hence, the specimen height was implicitly selected to vary in the range 1.12–1.20 m, as specified in Table 3.

**Table 3** L-shaped panel subassemblies—specimen nomenclature and test characteristics

Specimen #	Specimen type	Height (m)	Length (m)	Width (m)	Static scheme
08	L-20-12	1.20	1	2	Cantilever
09	L-20-20	1.20	1	2	Cantilever
10	L-12-20	1.12	1	2	Cantilever
11	L-12-12	1.12	1	2	Cantilever



Concrete class and steel type were assumed to be equal to those selected for wall systems, and the same applies to the criteria adopted for both anchorage detailing and joint execution (see Fig. 5). As described in Sect. 3.1, where the results of characterization tests are presented, concrete class C35/45 according to Eurocode 2 (CEN, European Committee for Standardization 2004a) was used for all precast subassemblies, while steel type B450C was used for both longitudinal and transverse reinforcement. Similarly, threaded M8 anchors made of steel grade 8.8 were provided as mechanical connectors of the two RC panels composing each specimen. To arrange panel-to-panel connections, two  $200 \times 150$  mm niches were settled into the inner edge of each panel and the hook reinforcement was directly anchored to the longitudinal bars through threaded bolts and steel plates (Fig. 5). The embedment depth of the two hooked anchor rods was once again selected to be approximately equal to 100 and 70 mm, according to panel thickness, and the joints were grouted up with the same type of mortar selected for wall systems. Its 28-day compressive strength was 15 MPa.

### 4.2 Test setup and loading protocol

A cantilevered static scheme was assumed to perform the set of asymmetric push–pull tests without initial axial load. As such, each specimen was set in place and post-tensioned to the strong floor of the laboratory through a stiff steel beam positioned at roughly two-thirds of the total panel length. To this aim,  $\varnothing 100$  channels were embedded at 350 mm from both panel edges, thus implying a channel-to-channel distance equal to 1300 mm. In single bending configuration, a MTS actuator was used to apply an asymmetric push–pull loading history in displacement control. As summarized in Table 4, twelve horizontal drift levels, consisting of  $\pm 0.1$ ,  $\pm 0.2$ ,  $\pm 0.4$ ,  $\pm 0.6$ ,  $\pm 0.8$ ,  $\pm 1.0$ ,  $\pm 1.5$ , 2.0, 3.0, 4.0, 5.0, and  $\pm 7.5\%$ , were imposed at the top of each specimen in quasi-static fashion. Three half cycles per amplitude were planned at a loading rate in the range 0.025–0.375 mm/s.

A schematic of typical specimen instrumentation installed to monitor absolute and relative displacements of key components is provided in Fig. 21. In particular,

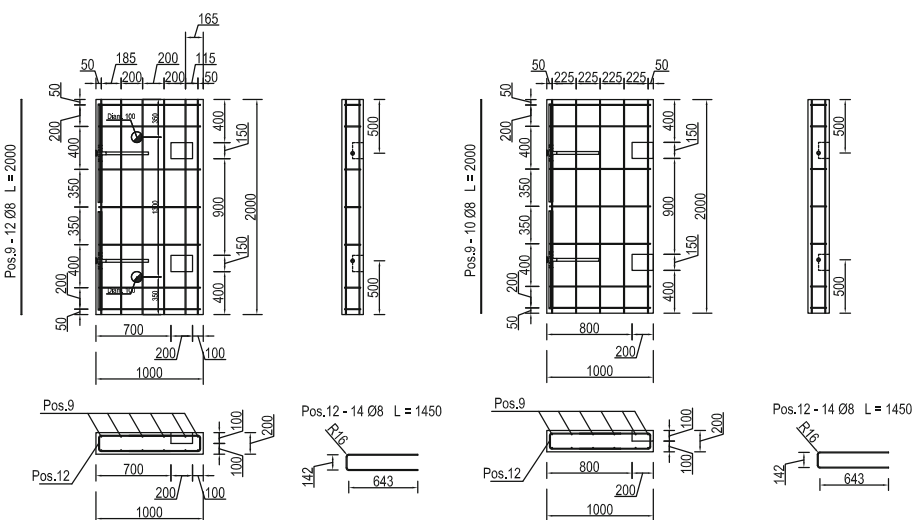


**Fig. 20** Example of reinforcement layout in panel subassemblies—specimen 09

displacement transducers labeled as 1(2) and 7(8) were arranged to measure lateral displacement at the top and bottom of the horizontal panels, respectively. In addition, slippage or uplift in the footing was monitored by linear potentiometers 3–6, while the set of sensors 9–14 measured any type of relative mechanism between the two panels.

### 4.3 Experimental response of case-study prototypes

The set of horizontal force–displacement capacity curves obtained for panel subsystems are shown in Fig. 22, while Fig. 23 provides representative observations in terms of deformed shapes, damage patterns and corresponding resisting mechanisms collected during the experimental program. Original unfiltered results were presented in this case so that a measure of the accuracy/inaccuracy of controllers and data acquisition systems can be associated with the experimental measurements, whether the level of applied forces is extremely low. Although spurious/fictitious components are negligibly small, a running average procedure (Psycharis and Mouzakis 2012a) can be used to filter and smoothen the response graphs discussed in the following.

In all asymmetric push–pull tests it was noticed that this type of pinned dry connections can accommodate large joint rotations of up to 0.075 rad without significant damage in panel segments. As a result of relative slippage and rigid rotation in the connection system, only a single net crack indeed formed at the base of each vertical panel and propagated along the entire width of the specimen (see Fig. 23). At the early stages of imposed loading history, a gap opened up in tension but closed in compression and, hence, one side of the bottom face lost contact with the underlying panel but the opposite side reseated and began to bear on it. During increasing cyclic reversals, the faying surfaces of each panel subsystem slipped over repeatedly, producing visible stiffness degradation and strength deterioration (Fig. 22). As such, the strength of all connection systems was observed to decrease with the number of applied cycles at each level of horizontal drift, which is mainly attributable to an increased local cracking of concrete around the dowels after each

**Table 4** Experimental loading protocol for panel subassemblies

Test #	Test name	Main DoF	Control type (force or displ.)	MAX ampl. (kN mm)	MIN ampl. (kN mm)	Loading speed (kN/s mm/s)	Load shape	Axial load (kN)	Cycles (#)
0	Axial	–	–	–	–	–	–	–	–
1	Drift #01	Long.	Displ.	1	0	0.025	Triang.	–	3
2	Drift #02	Long.	Displ.	2	0	0.050	Triang.	–	3
3	Drift #03	Long.	Displ.	4	0	0.100	Triang.	–	3
4	Drift #04	Long.	Displ.	6	0	0.150	Triang.	–	3
5	Drift #05	Long.	Displ.	8	0	0.150	Triang.	–	3
6	Drift #06	Long.	Displ.	10	0	0.150	Triang.	–	3
7	Drift #07	Long.	Displ.	15	0	0.150	Triang.	–	3
8	Drift #08	Long.	Displ.	20	0	0.150	Triang.	–	3
9	Drift #09	Long.	Displ.	30	0	0.150	Triang.	–	3
10	Drift #10	Long.	Displ.	40	0	0.200	Triang.	–	3
11	Drift #11	Long.	Displ.	50	0	0.250	Triang.	–	3
12	Drift #12	Long.	Displ.	75	0	0.375	Triang.	–	3

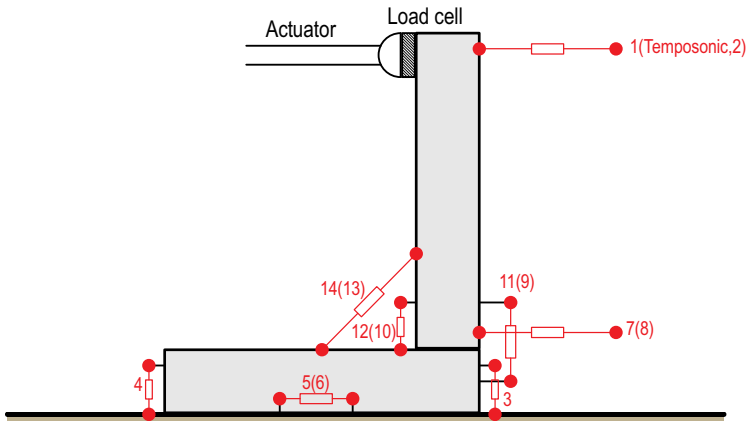


**Fig. 21** Experimental setup and instrumentation for each test on panel subsystems

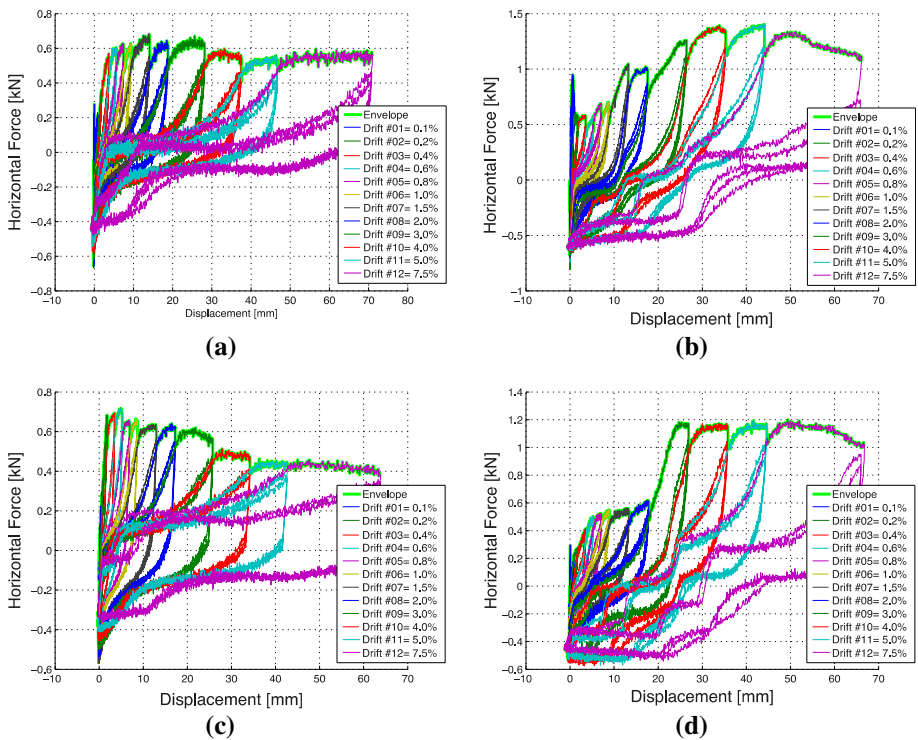


**Fig. 22** Asymmetric push–pull force–displacement curves of panel subsystems: **a** specimen 08; **b** specimen 09; **c** specimen 10; **d** specimen 11

cycle that resulted in a more pronounced relative slippage of threaded anchors. In case of specimen 08, the observed strength drop was around 20% in the second cycle and more than 25% in the third cycle, compared to the first one. Significant pinching was also observed, especially for horizontal drifts larger than 3, due to concrete cracking and consequent loosening of mechanical connectors. Accordingly, moderate energy dissipation

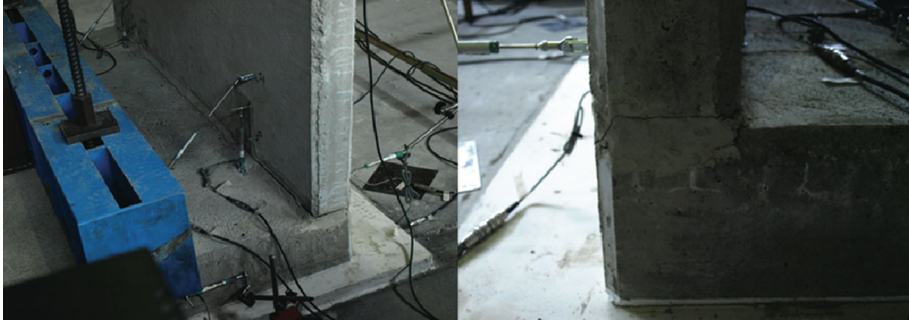


**Fig. 23** Deformed shapes at ultimate conditions and damage mechanisms of panel subsystems—specimen 08

was associated with this type of response and damage mechanisms. As shown in Fig. 22a, the envelope of lateral force–displacement curves presents gradual softening as the drift amplitude increases, and a similar behavior can be shown whether the set of peak capacities obtained from the second and third cycles are considered.

A more pronounced softening response was determined for specimen 10 (see Fig. 22c), while an opposite trend can be highlighted in case of specimens 09 and 11, as depicted in Fig. 22b, d respectively. In this latter case (i.e. 120–120 mm panel subassembly), a load pickup occurred at 3% drift cycles and the lateral capacity was observed to remain fairly constant after this level of imposed horizontal displacement. A similar but more gradual nonlinear regime can be shown by the envelope of experimental predictions obtained for specimen 09 (i.e. 200–200 mm panel subsystem), as the anticipated load pickup experienced during 1.5% drift cycles was combined with a more visible variation of horizontal load at increasing displacement amplitudes. Even if in some cases (e.g. specimens 08 and 10—see Fig. 22a, c) the hysteretic behavior was less poor than that observed in others (e.g. specimens 09 and 11—see Fig. 22b, d), all capacity curves revealed that the effects of slippage were pronounced and the loops were too unstable to develop a rationally controlled resisting mechanism. An almost negligible shear and bending moment transfer was found to take place between adjacent panels regardless of their thickness. In detail, moderate joint capacities in the range 0.7–1.4 kN were obtained experimentally for the set of complementary subsystems under investigation and, in addition, a low energy dissipation capacity was confirmed for this type of connection systems. In some cases, an evident stiffness degradation and strength deterioration dominated their cyclic response, particularly when the ultimate drift amplitude was applied to the specimen. Such an experimental outcome is therefore consistent with the assumption that this type of dry joints can be satisfactorily treated and modeled as a perfectly pinned connection system, in which a complete release of bending moments is imposed to occur between adjoining members in correspondence to the threaded anchors before their premature failure in shear.

## 5 Numerical simulation of precast wall systems

In the second stage of this research, specific modeling procedures for quick and accurate seismic response assessment of precast terraced buildings typical of past and current Dutch construction practice were defined and implemented, integrating mechanical idealizations and fiber-based approaches within a FE platform for nonlinear static analysis. Numerical

assumptions and computational strategies were discussed, and two-dimensional models of the tested precast walls were developed to study the response of this structural system at a global scale. The results of a set of geometrically and materially nonlinear simulations were presented in comparison with experimental estimates, quantifying the effectiveness of numerical predictions in relation to axial load increments and variations in the geometry (i.e. wall thickness and presence of openings) of these precast panels if subjected to in-plane shear and axial stresses (i.e. membrane elements). Comparisons may thus serve as a validation of this phenomenological macro modeling approach, making it applicable for large scale seismic fragility analysis of similar building classes.

## 5.1 Modeling approach and computational techniques

To reproduce the experimental behavior of the seven specimens presented in Sect. 3, simple mechanical models, consisting of inelastic fiber beam-column elements in combination with a set of nonlinear (i.e. bilinear) shear-flexural links, were constructed in SeismoStruct. In Fig. 24, an isometric view of the planar representation proposed for seismic analysis of these lightly reinforced precast concrete panels can be observed, while the prevailing assumptions concerning its implementation, formulation and calibration are discussed in the following.

Although geometric nonlinearities possibly play a weak role in the response of such wall systems, potential large displacements/rotations and P-Delta effects were taken into account using a total corotational transformation and, in addition, lumped-plasticity and distributed-plasticity approaches were combined to explicitly recognize different sources of material nonlinearity in this FE idealization. In particular, classical inelastic force-based fiber elements (Spacone et al. 1996), commonly used for damage analysis of concrete structures (Crowley et al. 2004; Silva et al. 2013; Brunesi and Nascimbene 2014; Brunesi et al. 2015a; Beyer et al. 2008), were assumed to model each wall segment of the panel assembly. As such, the spreading of inelasticity over the member length and cross section was reproduced through a direct integration of the uniaxial material response of individual fibers, which provided sectional stresses and strains at key positions of the wall member. Each inelastic beam-column element had five integration points and each cross section was discretized in four hundred fibers to accurately represent its stress/strain state during incremental monotonic loading. A simple bilinear constitutive rule with isotropic strain hardening was assigned to reinforcing steel, whereas the uniaxial uniform confinement model proposed by Mander et al. (1988) was assumed to simulate the inelastic behavior of concrete, explicitly accounting for tension softening. Furthermore, the response of wall-to-foundation and wall-to-wall connections was reproduced in a phenomenological sense by means of inelastic shear-flexural zero-length elements introduced to concentrate peculiar behavioral mechanism for such systems in specific portions of panel assembly. As shown in Fig. 24, a nonlinear link with bilinear shear and flexural constitutive relationships was provided at the base of each wall segment to allow for potential rocking and sliding of the panels relative to the foundation. Similarly, a one-to-three correspondence between structural members and model elements was assumed in such a way that infinitely rigid horizontal links and zero-length elements can be used to connect the two wall segments, reproducing flexural and shear response of panel-to-panel joints.

The flexural constitutive rule of nonlinear springs at the base was characterized by computing the overturning moment of the system according to basic stability principles (see Fig. 25), whereas the elastic stiffness of each wall segment was calculated by imposing a cantilever-like static scheme, as done during the test. Simple equilibrium

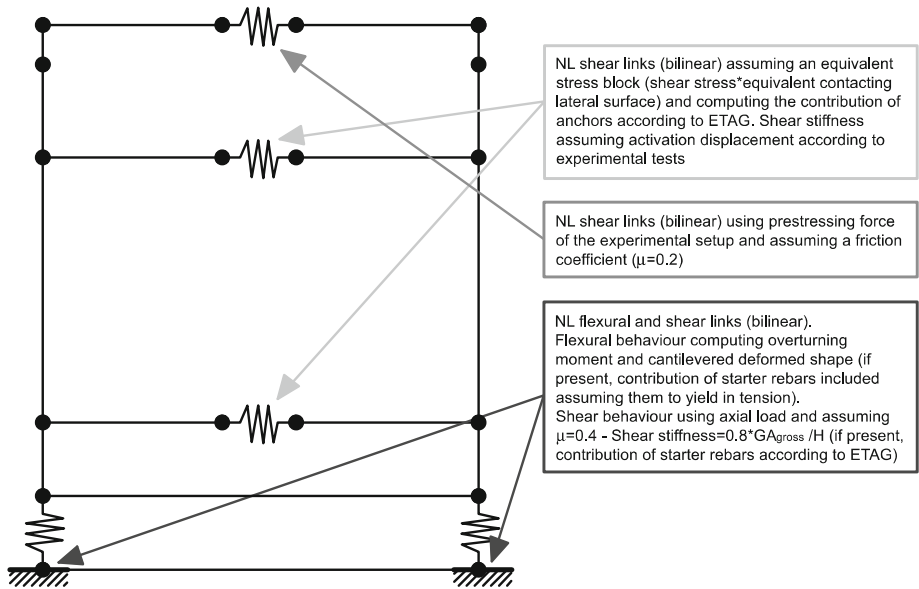


**Fig. 24** Example of mechanical FE idealization based on combined lumped-plasticity and distributed-plasticity approach—specimen 01

equations can be used to predict the activation of rocking mechanism, thus implementing it in a phenomenological sense. Considering that rocking takes place around the poles of rotation located close to the ends of the wall base, the horizontal force corresponding to the activation of this mechanism ( $F$ ) can be expressed as follows:

$$F = \frac{1}{H} N \frac{l}{2} \tag{1}$$

Alternatively, Eq. (1) can be reformulated in terms of bending moment ( $M$ ) simply using translational equilibrium along the vertical direction and assuming  $O'$  as the pole of rotation around which the mechanism occur:

$$M = N \left( \frac{l-a}{2} \right) = \frac{Nl}{2} \left( 1 - \frac{N}{k f_{cm} l t} \right) \tag{2}$$

where  $t$  is the wall thickness,  $f_{cm}$  is the compressive strength of concrete and  $k$  was set equal to 1 in this case, according to the shape of the equivalent stress block. Such an approach was considered to determine mechanical properties of flexural springs, taking into account the self-weight of the wall as well. If present, the contribution of starter rebars protruding from the foundation was included in the simulation assuming them to yield in tension. Furthermore, the shear behavior was obtained through a reduction of uncracked shear stiffness in accordance with past experimental studies (Beyer et al. 2008) and basic concepts of friction mechanics. As suggested by Beyer et al. (2008), the elastic properties of transverse springs were computed to represent the shear stiffness of uncracked sections in which the shear area was taken as 80% of the gross area, while a concrete-to-concrete friction coefficient ( $\mu$ ) equal to 0.4 was assumed to determine the activation force of sliding mechanisms. ETAG equations (EOTA, European Organization for Technical Approvals

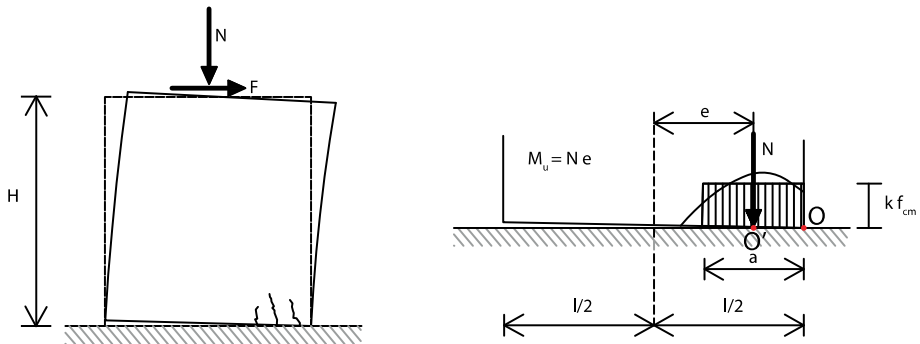


**Fig. 25** Activation of rocking and implementation of this mechanism in terms of equilibrium equations

2010) were considered to compute the shear strength of starter rebars, when provided at the base of panel assemblies. Nevertheless, it is worth mentioning that their effects were found to be minor either in terms of shear or flexural resistance, as also shown by experimental results.

As done in case of inelastic links at the base, flexural and shear mechanisms of wall-to-wall joints were decoupled. A perfect release of bending moment transfer between adjacent panels was imposed in accordance with experimental observations. Capacity curves and damage modes collected in Figs. 22 and 23 are in close agreement with this hypothesis, especially when considering that the rotation demand experienced by this type of structural walls at the level of panel-to-panel connections (Sect. 3.3) does not correspond to such a large drift amplitude. To reproduce shear behavior, a uniform stress block-based approach was prepared assuming an equivalent portion of the panel lateral surface as the contacting-contacted area of two adjacent walls across which the shear stresses were transferred during rocking mechanism. More in detail, a value of 3 MPa was considered, being the area equal to approximately one tenth of the lateral surface of the wall. As before, ETAG expressions (EOTA, European Organization for Technical Approvals 2010) were adopted to include the contribution of threaded anchor rods, even if similar considerations can be drawn in terms of their influence on shear resistance.

Very high stiffness was assigned to the top steel beams in order to minimize their interaction with the primary elements of the model and a friction-based inelastic shear link was additionally provided in between them to interrupt their continuity. Its calibration was carried out according to experimental data, in terms of activation displacement (i.e. 3 mm), prestressing force of test setup (i.e. 300 kN) and frictional properties of Teflon (i.e. 0.2).

A classical displacement/rotation-based convergence criterion, with a threshold set equal to  $10^{-3}$ , was assumed to perform the series of nonlinear static simulations using Hilber-Hughes-Taylor algorithm to iteratively equilibrate monotonically increased lateral loads. A summary of the analysis results is presented in the upcoming section, where monotonic capacity curves are compared to experimental data in order to demonstrate the effectiveness of this mechanical fiber-based macro-model concept for seismic fragility analysis of those buildings. Although other phenomenological approaches developed along the lines of classical multiple-vertical-line-element models or more recent multi-layer membrane element models were shown to be valid and viable methods to accurately simulate the behavior of wall systems (Ghobarah and Youssef 1999; Brunesi et al. 2016; Palermo and Trombetti 2016), a higher level of complexity and computational effort is

required, particularly if the response of entire structural prototypes has to be reproduced in a probabilistic fashion. In addition to that, higher computational costs are not necessarily associated with higher accuracy, particularly in case that minor damage occurs and the elongation of the neutral axis depth plays a weak role in the response (Priestley et al. 1999).

## 5.2 Monotonic static analysis versus cyclic pseudo-static tests

The simple numerical idealization proposed in this research was proven to be quite effective for computationally efficient response assessment of lightly reinforced precast concrete wall systems, whose damage modes and related resisting mechanisms were controlled by a complex interaction between shear and flexural behavior of their key components. An example of the deformed shape predicted for a representative panel assembly (i.e. specimen 01) is presented in Fig. 26, while a comparison between numerical and experimental horizontal force-drift curves is provided in Fig. 27. Rocking/sliding response and premature shear failure of wall-to-wall connections were reproduced numerically, thus reaffirming that joints designed without specific mechanical devices as seismic load transfer are the most vulnerable components of the system analyzed because of the displacement incompatibility between structural elements. Figure 26 illustrates the kinematics of this mechanism, which is in close agreement with experimental observations (see Fig. 9). As a result of this relative displacement incompatibility, unintended forces were attracted in poorly conceived and detailed connection systems that primarily rely on shear friction. Given that threaded anchor rods were characterized by an intrinsic lack of shear and ductility capacity, the concentration of strain and force demand at the connection level due to the greater flexibility of the joints (compared with the connected precast concrete walls) was shown to cause this type of severe local damage under earthquake-induced lateral loads.

Considering the 200 mm thick wall system (see Fig. 27a), quite accurate predictions can be observed in terms of peak load bearing capacity. In detail, a maximum of approximately 326 kN was obtained for specimen 01, showing an experimental-to-numerical resistance ratio ( $R$ ) equal to 1.02. A similar consideration can be drawn in case of 120 mm thick panel assemblies without any opening in their structural layout (see Fig. 27b), as a peak value of up to 202 kN was determined for specimen 02, thus implying  $R$  to be equal to 1.04. It is worthwhile to note that the first cycle of 1.0% drift amplitude was assumed herein to compute the ratios between experimentally observed and numerically predicted load carrying capacities, as no fictitious resistance overestimates were measured at this lateral displacement level due to the test setup (see Sect. 3.3).

By contrast, slightly different trends were obtained for wall prototypes presenting an opening in their geometry. As far as specimens with a door are concerned, a further force-based fiber element was introduced at the center line of the lintel; the depth of its cross section equals the height of the lintel and the width equals the thickness of the wall. A similar approach was also assumed for the presence of a window, considering an additional inelastic beam-column element underneath it. In this latter case (see Fig. 27c), the model was observed to reproduce the stiffness reduction caused by the presence of a window, as well as the formation of initial cracks in correspondence to the corners of the opening. A satisfying match with experimental lateral load capacities was achieved up to 0.8% drift cycles, as a maximum resistance of approximately 271 kN was determined numerically, resulting in a more conservative but slightly less accurate fit than that highlighted in case of structural wall systems without openings. When compared to those panel assemblies, a more than double mismatch was computed, being  $R$  equal to approximately 1.14.



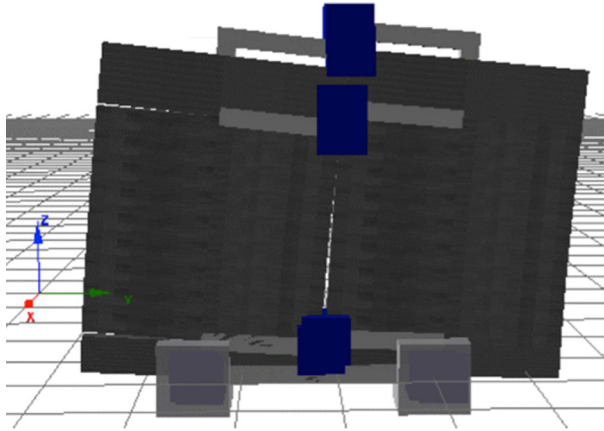


**Fig. 26** Extruded view of deformed shape predicted for a representative structural wall system—specimen 01

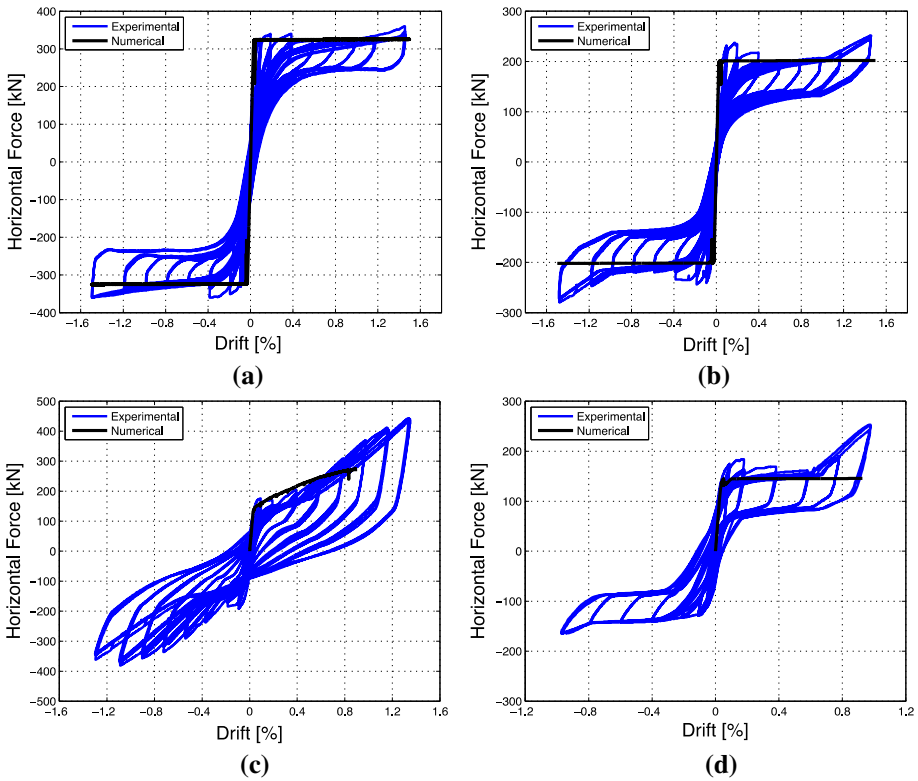


**Fig. 27** Comparison between experimental and numerical predictions: **a** specimen 01; **b** specimen 02; **c** specimen 04; **d** specimen 06

Furthermore, the discrepancy between numerical and experimental estimates was shown to increase as the lateral displacement increased and damage propagated into the panel up to the final buckling of the longitudinal reinforcing rebars. Hence, this mechanical fiber-based approach is beyond the purposes of its application for larger drift amplitudes, in which the response of the wall assembly was mainly dominated by the evolution of strut and tie mechanisms that can be conversely taken into account through detailed two-dimensional shell or three-dimensional solid models (Todut et al. 2014; Palermo and Trombetti 2016).

Compared to solid wall systems, an almost identical accuracy can be observed in case of specimens presenting a door (Fig. 27d), considering that a difference of up to 7% was obtained. More in detail, a peak lateral resistance of about 146 kN was predicted for specimen 06 at horizontal displacements roughly equal to 18 mm. Even in this case, the increment of horizontal capacity recorded for larger drifts was attributable to the spurious vertical component due to the actuator misalignment, which in turn was associated with the rocking response of this prototype. Such a mechanism resulting in panel detaching and shear/buckling failure of anchors was once again predicted to occur in close correlation with the experimental damage patterns shown in Fig. 16.

A substantial agreement between experimental and numerical resistance estimates can be therefore reaffirmed, whether specimens with or without openings are considered. In particular,  $R$  in the range 1.02–1.14 was indeed determined, with an average of about 1.07 and a moderate standard deviation roughly equal to 4%. In light of the aforementioned considerations, this type of mechanical fiber-based idealization, in compliance with experimental validation to ensure that all possible failure modes are taken into account, appears to be a viable and promising technique for seismic analysis of such structural wall systems at a global scale. Accordingly, such an approach can be immediately applied and extended to predict global-structural variations in their seismic response as a consequence of local parametric changes in their configuration following peculiar geometrical features of their layout. The proposed mechanical/phenomenological representation can be therefore integrated in a framework for pushover-based fragility analysis of this type of building classes. Several contributions constitute the theoretical background for selecting this method of analysis as a reliable tool for large scale vulnerability assessment of structures [see among others (Crowley et al. 2004; Silva et al. 2013; Antoniou and Pinho 2004)], and hence the modeling techniques shown and validated in this paper are primarily concerned with the use of monotonic nonlinear static simulation procedures. Despite this, the same macro-model concept described here can be implemented into flag-shape constitutive laws in order to reproduce the cyclic response of similar structures, in case that nonlinear dynamic analysis is assumed as a favorite approach for numerical simulation.

Of paramount importance is, in this latter case, the constitutive rule selected to model the dynamic behavior of rocking walls, due to the fact that the stiffness change typical of elastic bilinear and flag-shape hysteresis may result in acceleration spikes arising when the wall base gap closes. This phenomenon has been previously observed in numerical simulations and experimental tests (Rodríguez et al. 2002; Toranzo et al. 2009; Wiebe and Christopoulos 2010; Belleri et al. 2014), and it may cause an increase of the base shear demand at lower than expected wall base rotations. In particular, Wiebe and Christopoulos (Wiebe and Christopoulos 2010) have demonstrated that acceleration spikes are likely to occur in nonlinear springs that are initially fairly rigid, particularly when those springs change from low stiffness to high stiffness while moving at a high velocity. Accordingly, it was concluded that accelerations at changes in stiffness are caused by physical phenomena, such as the combination of wall rotational velocity and system lateral stiffness, but may be amplified by modeling decisions. Along this line, Fig. 28 presents the results of a

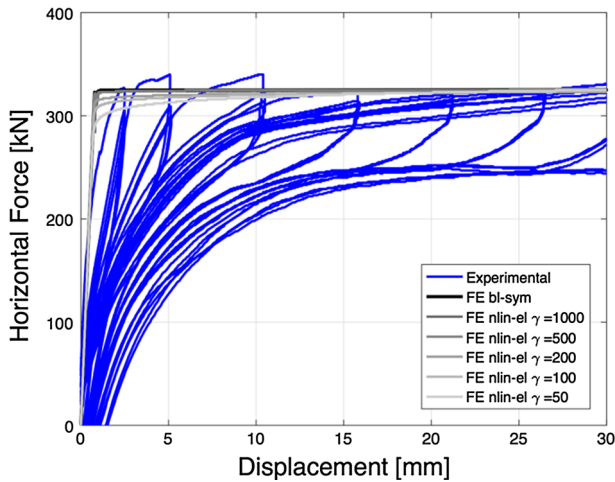


**Fig. 28** Parametric analysis: bl-sym model versus nlin-el model—specimen 01

parametric study showing that use can be made of more refined constitutive laws (i.e. nlin-el model) to smoothen the sharp change in stiffness that is, by definition, associated with bilinear rules, namely bl-sym. As suggested by Kaldjian (1967) and implemented by Otani (1981), the rounded curve of the Ramberg–Osgood model adopted in Fig. 28 can be defined as follows:

$$\frac{R_i}{R} = \frac{M_i}{M} \left( 1 + \left| \frac{M_i}{M} \right|^{\gamma-1} \right) \tag{3}$$

where  $M_i$  and  $R_i$  are the moment and rotation at the  $i$ th step,  $M$  and  $R$  are the activation moment and rotation, and  $\gamma$  is the Ramberg–Osgood parameter, which was assumed to vary in the range 1000–50.

## 6 Conclusions

The experimental and numerical research described here was conducted to investigate the seismic behavior of lightly reinforced precast concrete wall systems common in northern European regions that are characterized by little or no natural seismicity. Seven full-scale RC panel assemblies typical of low- to mid-rise precast residential multi-unit terraced buildings stricken by induced earthquakes in the Groningen region were tested under pseudostatic in-plane cyclic loading in order to assess their performance at progressively increasing seismic intensities. Trends were discussed in terms of damage modes and hysteretic capacity curves, and upper/lower bounds for lateral load resistance of such wall systems were provided, assuming compressive axial forces comparable to those exerted in practice. The response of specimens with and without openings (i.e. doors and windows) were then compared so as to explore their influence on structural integrity of the system tested, as well as to quantify their interaction with respect to the global response of the reference solid wall assemblies and with respect to the local performance of the joints. The

prevailing observations and conclusions, drawn from this experimental study, are summarized as follows:

- Behavioral changes as a consequence of variations in initial axial load and wall geometry (i.e. panel thickness and presence of openings) were investigated, permitting an extensive evaluation of local seismic vulnerabilities that occurred in poorly conceived and detailed connection systems designed without the ability to accommodate relative displacements between structural precast members. All specimens were found to collapse by a premature shear failure of their panel-to-panel joints, which were proven to be the weakest link of the wall systems tested, and this aspect is a key consideration towards the improvement of their early design.
- Resisting mechanisms and related damage modes were examined, revealing that rocking/sliding response was primarily associated with shear-buckling failure of threaded anchor rods and minor concrete spalling/crushing at the base of each wall segment, regardless of its thickness. Except for the latter occurrence, no damage was observed in lightly reinforced precast concrete elements and the prevailing source of material nonlinearity was in the response of the joints due to a combination of slip and damage to their components. This behavior was particularly evident in case of prototypes without openings in their layout.
- In case of structural cutouts, the classical base uplift resulting from rocking behavior of the panel assembly was associated with the formation and propagation of visible horizontal and diagonal cracks at the bottom corners of the window and in correspondence to the top right free corner of the door, which finally caused a pronounced local buckling of the longitudinal reinforcing rebars provided at the edges of the opening. Therefore, more dissipative and stable hysteresis loops obtained for walls presenting a window in their structural layout were opposed to narrow thin-shaped cycles with moderate and gradual strength degradation in case of solid panels dominated mostly by rocking mechanisms.
- Such a behavior additionally contrasted with a more complex hybrid response experienced by prototypes with a door, in which it was shown a more significant interaction between geometric and material sources of nonlinearity (i.e. rocking and plasticity), thus implying hysteretic cycles slightly more weakened in character than those observed in the former case. As a result, different levels of stiffness degradation and strength deterioration can be found for this type of cantilevered precast wall systems, depending on panel geometry (i.e. wall thickness and different opening configurations) and initial condition (i.e. axial load), as well as drift amplitudes and number of cycles.

Furthermore, displacement-controlled asymmetric push–pull tests of four panel sub-systems with variable wall thickness were performed to specifically characterize the seismic performance of dry joint systems, providing additional data for numerical modeling. The main conclusions, drawn from this complementary set of experimental tests, can be summarized as follows:

- All tests confirmed that an almost negligible shear and bending moment transfer was observed to take place in such connections which were proven to accommodate large joint rotations without significant damage in panel segments.
- Accordingly, local concrete cracking and consequent loosening of mechanical connectors governed the experimental response of each complementary specimen under investigation, regardless of the wall thickness.

- Visible pinching and low energy dissipation capacity were shown for this type of connection systems that revealed an evident stiffness degradation and strength deterioration with the drift amplitude and the number of applied cycles for a given level of lateral displacement.

Numerical models able to account for material and geometric nonlinearities were also developed within a FE platform for nonlinear static analysis, using inelastic force-based fiber elements to model wall members and mechanical idealizations to reproduce the shear-flexural behavior of wall-to-wall and wall-to-foundation connections in a phenomenological sense. These conclusions can be derived from the series of numerical analyses carried out:

- Monotonic predictions were compared to the experimental results obtained for the seven full-scale wall systems tested here, demonstrating the effectiveness of this FE representation for computationally efficient seismic response assessment of lightly reinforced precast concrete bearing panels of this particular type.
- In light of this, such a methodology, in compliance with the experimental outcome of the research, may be immediately extended to vulnerability assessment, fragility analysis and retrofit of precast RC terraced buildings representative of those used for housing in the Netherlands.
- Further experimental investigation, which is currently the focus of the on-going research, may be desirable for an additional validation of the proposed numerical idealization. More in detail, dynamic shake table tests and pseudo-static cyclic tests on twin two-story full-scale specimens are in progress and they can be referred to as the major activities of an exhaustive experimental research program. Tests on both entire full-scale building prototypes and other structural components/members may thus be used for this purpose and they may also serve as a cross-validation/extension of the experimental trends emerged and discussed in the present paper.

**Acknowledgements** This paper describes an activity that is part of the “Numerical and experimental evaluation of the seismic response of precast wall connections” project at Eucentre, undertaken within the framework of the research program for hazard and risk of induced seismicity in Groningen sponsored by the Nederlandse Aardolie Maatschappij BV. The authors would like to thank all the parties involved in this project: DICAr Lab of University of Pavia and Eucentre Lab that performed the test, together with NAM, Arup and TU Delft. Moreover, the authors are deeply indebted to Prof. Alberto Pavese, Dr. Filippo Dacarro and Dr. Simone Peloso for the extensive comments given on this research. Lastly, the authors are sincerely thankful to Dr. Giulia Fagà for the insightful support with figure editing.

## References

- Antoniou S, Pinho R (2004) Development and verification of a displacement-based adaptive pushover procedure. *J Earthq Eng* 8(5):643–661
- Belleri A, Riva P (2012) Seismic performance and retrofit of precast grouted sleeve connections. *PCI J* 57(1):97–109
- Belleri A, Schoettler MJ, Restrepo JJ, Fleischman RB (2014) Dynamic behavior of rocking and hybrid cantilever walls in a precast concrete building. *ACI Struct J* 111(3):661–671
- Belleri A, Brunesi E, Nascimbene R, Pagani M, Riva P (2015) Seismic performance of precast industrial facilities following major earthquakes in the Italian territory. *J Perform Constr Facil ASCE* 29(5):04014135
- Belleri A, Torquati M, Marini A, Riva P (2016) Horizontal cladding panels: in-plane seismic performance in precast concrete buildings. *Bull Earthq Eng* 14(4):1103–1129

- Beyer K, Dazio A, Priestley MJN (2008) Inelastic wide-column models for U-shaped reinforced concrete walls. *J Earthq Eng* 12(S1):1–33
- Biondini F, Dal Lago B, Toniolo G (2013) Role of wall panel connections on the seismic performance of precast structures. *Bull Earthq Eng* 11(4):1061–1081
- Bommer JJ, Crowley H, Pinho R (2015) A risk-mitigation approach to the management of induced seismicity. *J Seismol* 19(2):623–646
- Bournas DA, Negro P, Molina FJ (2013) Pseudodynamic tests on a full-scale 3-storey precast concrete building: behavior of the mechanical connections and floor diaphragms. *Eng Struct* 2013(57):609–627
- Brunesi E, Nascimbene R (2014) Extreme response of reinforced concrete buildings through fiber force-based finite element analysis. *Eng Struct* 69:206–215
- Brunesi E, Nascimbene R, Bolognini D, Bellotti D (2015a) Experimental investigation of the cyclic response of reinforced precast concrete framed structures. *PCI J* 60(2):57–79
- Brunesi E, Nascimbene R, Deyanova M, Pagani C, Zambelli S (2015b) Numerical simulation of hollow steel profiles for lightweight concrete sandwich panels. *Comput Concr* 15(6):951–972
- Brunesi E, Nascimbene R, Parisi F, Augenti N (2015c) Progressive collapse fragility of reinforced concrete framed structures through incremental dynamic analysis. *Eng Struct* 104:65–79
- Brunesi E, Nascimbene R, Pavese A (2016) Mechanical model for seismic response assessment of lightly reinforced concrete walls. *Earthq Struct* 11(3):461–481
- CEN, European Committee for Standardization (2004a) EN 1992-1-1. Eurocode 2 (EC2): design of concrete structures—part 1.1: general rules and rules for buildings. Brussels, Belgium
- CEN, European Committee for Standardization (2004b) EN 1998-1-5. Eurocode 8 (EC8): design of structures for earthquake resistance—part 1.5: specific rules for concrete buildings. Brussels, Belgium
- Crisafulli FJ, Restrepo JJ, Park R (2002) Seismic design of lightly reinforced precast rectangular wall panels. *PCI J* 47(4):104–121
- Crowley H, Pinho R, Bommer JJ (2004) A probabilistic displacement-based vulnerability assessment procedure for earthquake loss estimation. *Bull Earthq Eng* 2(2):173–219
- Dal Lago B, Toniolo G, Lamperti Tornaghi M (2016) Influence of different mechanical column-foundation connection devices on the seismic behaviour of precast structures. *Bull Earthq Eng* 14(12):3485–3508
- Dal Lago B, Biondini F, Toniolo G (2017a) Experimental investigation on steel W-shaped folded plate dissipative connectors for horizontal precast concrete cladding panels. *J Earthq Eng*. doi:[10.1080/13632469.2016.1264333](https://doi.org/10.1080/13632469.2016.1264333)
- Dal Lago B, Biondini F, Toniolo G, Lamperti Tornaghi M (2017b) Experimental investigation on the influence of silicone sealant on the seismic behaviour of precast façades. *Bull Earthq Eng* 15(4):1771–1787
- Dazio A, Beyer K, Bachmann H (2009) Quasi-static cyclic tests and plastic hinge analysis of RC structural walls. *Eng Struct* 31:1556–1571
- De Borst R (1987) Smear cracking, plasticity, creep and thermal loading—a unified approach. *Comp Meth Appl Mech Eng* 62(1):89–110
- Englekirk RE (2003) *Seismic design of reinforced and precast concrete buildings*. Wiley, New York
- EOTA, European Organization for Technical Approvals (2010) ETAG 001: guideline for european technical approval of metal anchors for use in concrete—annex C: design methods for anchorages. Brussels, Belgium
- Fédération Internationale du Béton (fib), Bulletin 43 (2008) *Structural connections for precast concrete buildings*. Lausanne, Switzerland: fib, federation internationale du béton
- Fintel M (1995) Performance of buildings with shear walls in earthquakes in the last thirty years. *PCI J* 4(3):62–80
- Fischinger M, Kramar M, Isakovic T (2008) Cyclic response of slender RC columns typical of precast industrial buildings. *Bull Earthq Eng* 6(3):519–534
- Ghobarah A, Youssef M (1999) Modelling of reinforced concrete structural walls. *Eng Struct* 21(10):912–923
- Hidalgo PA, Ledezma CA, Jordan RM (2002) Seismic behavior of squat reinforced concrete shear walls. *Earthq Spectra* 18(2):287–308
- Holden T, Restrepo J, Mander JB (2003) Seismic performance of precast reinforced and prestressed concrete walls. *J Struct Eng ASCE* 129(3):286–296
- Hung C-C, El-Tawil S (2010) Hybrid rotating/fixed-crack model for high performance fiber reinforced cementitious composites. *ACI Mater J* 107(6):568–576
- Kaldjian MJ (1967) Moment-curvature of beams as Ramberg-Osgood functions. *J Struct Div ASCE* 93(ST5):53–65
- Kang S-M, Kim O-J, Park H-G (2013) Cyclic loading test for emulative precast concrete walls with partially reduced rebar section. *Eng Struct* 56:1645–1657

- Kurama Y, Sause R, Pessiki S, Lu LW (1999) Lateral load behavior and seismic design of unbonded post-tensioned precast concrete walls. *ACI Struct J* 96(4):622–632
- Li B, Qian K, Wu H (2016) Flange effects on seismic performance of reinforced concrete squat walls with irregular or regular openings. *Eng Struct* 110:127–144
- Magliulo G, Ercolino M, Petrone C, Coppola O, Manfredi G (2014) The Emilia earthquake: seismic performance of precast reinforced concrete buildings. *Earthq Spectra* 30(2):891–912
- Magliulo G, Ercolino M, Manfredi G (2015) Influence of the cladding panels on the first period of one-storey precast building. *Bull Earthq Eng* 13(5):1531–1555
- Mander JB, Priestley MJN, Park R (1988) Theoretical stress-strain model for confined concrete. *J Struct Eng ASCE* 114(8):1804–1826
- Mousavi SA, Zahrai SM, Bahrami-Rad A (2014) Quasi-static cyclic tests on super-lightweight EPS concrete shear walls. *Eng Struct* 65:62–75
- Nederlands Normalisatie-instituut (2011) National annex to NEN-EN 1990 + A1 + A1/C2: eurocode: basis of structural design. Delft, the Netherlands
- Otani S (1981) Hysteresis models of reinforced concrete for earthquake response analysis. *J Fac Eng* 36(2):407–441
- Palermo M, Trombetti T (2016) Experimentally-validated modelling of thin RC sandwich walls subjected to seismic loads. *Eng Struct* 119:95–109
- Palermo M, Gil-Martín LM, Trombetti T, Hernandez-Montes E (2013) In-plane shear behaviour of thin low reinforced concrete panels for earthquake reconstruction. *Mater Struct* 46(5):841–856
- Palermo M, Ricci I, Silvestri S, Gasparini G, Trombetti T, Foti D, Ivorra S (2014) Preliminary interpretation of shaking-table response of a full-scale 3-storey building composed of thin reinforced concrete sandwich walls. *Eng Struct* 76:75–89
- Pavese A, Bournas DA (2011) Experimental assessment of the seismic performance of a prefabricated concrete structural wall system. *Eng Struct* 33:2049–2062
- Peng Y-Y, Qian J-R, Wang Y-H (2016) Cyclic performance of precast concrete shear walls with a mortar-sleeve connection for longitudinal steel bars. *Mater Struct* 49(6):2455–2469
- Priestley MJN, Sritharan SS, Conley JR, Pampanin S (1999) Preliminary results and conclusions from the PRESSS five-storey precast concrete test building. *PCI J* 44(6):42–67
- Psycharis IN, Mouzakis HP (2012a) Shear resistance of pinned connections of precast members to monotonic and cyclic loading. *Eng Struct* 41:413–427
- Psycharis IN, Mouzakis HP (2012b) Assessment of the seismic design of precast frames with pinned connections from shaking table tests. *Bull Earthq Eng* 10(6):1795–1817
- Rezaifar O, Kabir MZ, Taribakhsh M, Tehrani A (2008) Dynamic behaviour of 3D panel single-storey system using shaking-table testing. *Eng Struct* 30:318–337
- Ricci I, Palermo M, Gasparini G, Silvestri S, Trombetti T (2013) Results of pseudo-static tests with cyclic horizontal load on cast in situ sandwich squat concrete walls. *Eng Struct* 54:131–149
- Rodríguez M, Blandón J (2005) Tests on a half-scale two-storey seismic-resisting precast concrete building. *PCI J* 50(1):94–114
- Rodríguez ME, Restrepo JI, Carr AJ (2002) Earthquake-induced floor horizontal accelerations in buildings. *Earthq Eng Struct Dyn* 31(3):693–718
- Salonikios TN, Kappos AJ, Tegos IA, Penelis GG (1999) Cyclic load behavior of low-slenderness R/C walls: design basis and test results. *ACI Struct J* 96(4):649–660
- Salonikios TN, Kappos AJ, Tegos IA, Penelis GG (2000) Cyclic load behavior of low-slenderness R/C walls: failure modes, strength and deformation analysis, and design implications. *ACI Struct J* 97(1):132–141
- Seissoft (2016) SeismoStruct—a computer program for static and dynamic nonlinear analysis of framed structures. URL: [www.seissoft.com](http://www.seissoft.com)
- Silva V, Crowley H, Pinho R, Varum H (2013) Extending displacement-based earthquake loss assessment (DBELA) for the computation of fragility curves. *Eng Struct* 56:343–356
- Spacone E, Filippou FC, Taucer FF (1996) Fibre beam-column model for non-linear analysis of RC frames: part I. Formulation. *Earthq Eng Struct Dyn* 25:711–725
- Todut C, Dan D, Stoian V (2014) Theoretical and experimental study on precast reinforced concrete wall panels subjected to shear force. *Eng Struct* 80:323–338
- Toranzo LA, Restrepo JI, Mander JB, Carr AJ (2009) Shake-table tests of confined-masonry rocking walls with supplementary hysteretic damping. *J Earthq Eng* 13(6):882–898
- Tsoukantas SG, Tassios TP (1989) Shear resistance of connections between reinforced concrete linear precast elements. *ACI Struct J* 86(3):242–249
- Vintzeleou EN, Tassios TP (1987) Behavior of dowels under cyclic deformations. *ACI Struct J* 84(1):18–30

- Wiebe L, Christopoulos C (2010) Characterizing acceleration spikes due to stiffness changes in nonlinear systems. *Earthq Eng Struct Dyn* 39(14):1653–1670
- Zoubek B, Fischinger M, Isaković T (2016) Cyclic response of hammer-head strap cladding-to-structure connections used in RC precast building. *Eng Struct* 119:135–148